Nam *et al. Soft Sci* 2023;3:28
DOI: 10.20517/ss.2023.19

Soft Science

Review Article

Open Access

Check for updates

Soft conductive nanocomposites for recording biosignals on skin

Seonghyeon Nam[1,2,#], Chansul Park[1,2,#], Sung-Hyuk Sunwoo[1,2,3,#], Minseong Kim[1,2], Hyunjin Lee[1,2], Mincheol Lee[4,*], Dae-Hyeong Kim[1,2,5,*]

[1]Center for Nanoparticle Research, Institute for Basic Science (IBS), Seoul 08826, Republic of Korea.
[2]School of Chemical and Biological Engineering, Seoul National University, Seoul 08826, Republic of Korea.
[3]Institute of Radiation Medicine, Seoul National University Medical Research Center, Seoul 03080, Republic of Korea.
[4]Electro-Medical Equipment Research Division, Korea Electrotechnology Research Institute (KERI), Ansan 15588, Republic of Korea.
[5]Department of Materials Science and Engineering, Seoul National University, Seoul 08826, Republic of Korea.
[#]The authors contributed equally.

[*]**Correspondence to:** Prof. Dae-Hyeong Kim, School of Chemical and Biological Engineering, Seoul National University, 1, Gwanak-ro, Gwanak-gu, Seoul 08826, Republic of Korea. E-mail: dkim98@snu.ac.kr; Dr. Mincheol Lee, Electro-Medical Equipment Research Division, Korea Electrotechnology Research Institute (KERI), 111, Hanggaul-ro, Sangnok-gu, Ansan 15588, Republic of Korea. E-mail: minckeri@keri.re.kr

How to cite this article: Nam S, Park C, Sunwoo SH, Kim M, Lee H, Lee M, Kim DH. Soft conductive nanocomposites for recording biosignals on skin. *Soft Sci* 2023;3:28. https://dx.doi.org/10.20517/ss.2023.19

Received: 27 Apr 2023 **First Decision:** 1 Jun 2023 **Revised:** 21 Jun 2023 **Accepted:** 29 Jun 2023 **Published:** 2 Aug 2023

Academic Editor: Zhifeng Ren **Copy Editor:** Pei-Yun Wang **Production Editor:** Pei-Yun Wang

Abstract

Soft conductive nanocomposites have introduced significant breakthroughs in bio-integrated electronics by mitigating the mechanical mismatch between the body and the device. Compared with conventional wearable sensors based on rigid electronic materials, the wearable sensors based on soft nanocomposites are advantageous to long-term and high-quality biosignal recordings. Materials used for the synthesis of the nanocomposites, especially nanofillers, are critical for determining the quality of recorded biosignals and the performance of the nanocomposites. In this review, we focus on recent advances in soft conductive nanocomposites, mainly on their electrical and mechanical properties according to the types of nanofillers, and present their applications to wearable biosignal recording devices. We have classified the nanofillers into four categories: carbon-based nanomaterials, conducting polymers, metal-based nanomaterials, and liquid metals. We then introduce the applications of nanocomposites as wearable sensors that record various biosignals, including electrophysiological, strain, pressure, and biochemical information. In conclusion, a brief outlook on the remaining challenges for future nanomaterial-based bioelectronics is provided.

Keywords: Nanocomposites, nanomaterials, soft materials, wearable sensors, bio-integrated electronics

INTRODUCTION

Recording biosignals and analyzing the recorded data are prevalent not only by medical experts in clinics[1-3] but also by home users in their daily lives[4-6]. Accordingly, wearable electronic devices that record various physiological and electrophysiological signals, such as blood pressure (BP)[7], respiration rate[8], electrocardiogram (ECG)[9-11], electromyogram (EMG)[12], and electroencephalogram (EEG)[13,14], have been widely used for personalized health monitoring and disease diagnosis and treatment[11,15]. Providing precise and comprehensive information about the health condition of users is a key requirement for such devices. However, conventional rigid devices have difficulties interfacing with soft skin, which leads to a low signal-to-noise ratio (SNR) in biosensing and causes various side effects, including skin irritations[16], inflammatory responses[17,18], and user discomfort[19,20]. Additionally, accumulated mechanical stress can also degrade the materials of the devices, particularly those on the device surface, which may release harmful chemicals and trigger skin problems[21,22]. Therefore, breakthroughs in material and device design are necessary to enable long-term and high-quality biosignal recordings.

To achieve performance improvements in wearable biosignal recording devices, a completely new approach is necessary, such as adopting intrinsically soft materials instead of conventional rigid electronic materials. Rigid materials, such as metals and silicon, have high Young's moduli in the range of ~100 GPa[23], which are significantly higher than that of human skin (~1 MPa)[24,25] by orders of magnitude. On the other hand, soft materials, such as hydrogels (modulus range: 0.01 kPa-5 MPa)[26-30] and elastic polymers (modulus range: 50 kPa-50 MPa)[9,31,32], can achieve low Young's moduli for the fabricated devices, making their mechanical properties analogous to the soft, dynamic, and curvilinear human body. This would result in highly effective biosignal recordings with conformal integration with the skin and reduction of the aforementioned side effects.

To fabricate soft conductive materials and their devices, conductive materials should be incorporated as functional fillers into the soft elastomeric matrix. In particular, nanoscale conductive fillers are preferred, as they can impart electrical conductivity to their nanocomposites without compromising their softness[33]. These nanofillers can be homogeneously dispersed in the soft media to form a highly percolated network that maintains a seamless connection even when they are stretched. This property endows the nanocomposites with electrical conductivity under mechanical deformations, allowing for the efficient capture and noise-free transportation of biosignals[34-36]. By selecting appropriate nanofillers, the nanocomposites can further achieve a low contact impedance[37,38] and high chemical stability[39]. Therefore, it is worth considering nanofillers of different dimensions (e.g., 0D, 1D, and 2D) and various material types (e.g., carbon, polymer, and metal) to optimize the mechanical and electrical properties of the nanocomposites, aiming for high-performance wearable electronic devices.

In this article, we explore the latest developments in soft conductive nanocomposites and their applications in on-skin biosignal recording devices [Figure 1]. Firstly, we begin by categorizing the nanocomposites into four groups depending on the material types of nanofillers employed: carbon-based nanomaterials, conducting polymers (CPs), metal-based nanomaterials, and liquid metals (LMs). We then present detailed strategies for maximizing the performance of each nanofiller and its corresponding nanocomposite. Secondly, we categorize wearable biosignal recording devices into electrophysiological sensors, strain sensors, pressure sensors, and biochemical sensors, depending on the target biosignals. We analyze how each device category utilizes different types of nanocomposites to meet specific signal sensing requirements. Finally, we describe the remaining challenges that need to be addressed to further develop nanocomposites for practical applications in biosignal recording devices.

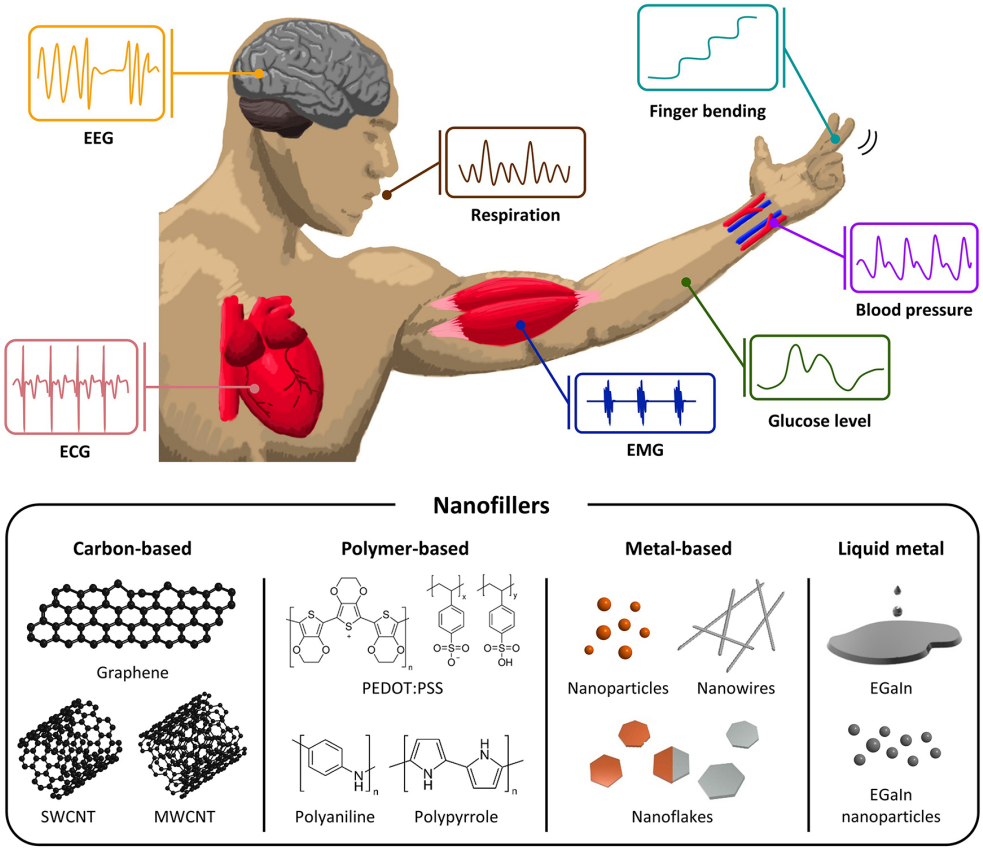

Figure 1. Schematics depicting various biosignals recorded by wearable devices and commonly used nanofillers for soft conductive nanocomposites. ECG: Electrocardiogram; EEG: electroencephalogram; EGaIn: eutectic gallium-indium; EMG: electromyogram; MWCNT: multi-walled carbon nanotube; PEDOT:PSS: poly(3,4-ethylenedioxythiophene):poly(styrene sulfonate); SWCNT: single-walled carbon nanotube.

NANOSCALE FILLERS FOR SOFT CONDUCTIVE NANOCOMPOSITES

As the way nanofillers assemble and form a percolated network inside elastic matrices decides the electrical properties of nanocomposites, it is important to determine the effect of their distribution and geometry on the performance of the nanocomposites, especially for high-quality biological signal sensing[16,33]. The percolation threshold, which is defined as the minimum volume fraction of nanoscale fillers required to form a long-range connectivity inside the nanocomposites, serves as a reference point for the nanocomposites to exhibit electrical conductivity. A small volume change of the filler near the percolation threshold can lead to a sudden transition of the electrical property between an insulator and a conductor[40], and a rapid enhancement of the conductivity can be achieved by embedding more conductive fillers beyond the percolation threshold.

However, excessive filler amounts lead to their aggregation, increase mechanical stiffness, and result in high costs. Therefore, modifying the characteristics and maximizing the performance of the nanocomposites by changing the volume fraction of the filler alone has limitations. Instead, controlling the types of filler materials and their morphologies can be a more effective way to tune the electrical properties of the nanocomposites. For instance, metal-based nanomaterials have higher intrinsic electrical conductivities compared to other types of nanomaterials[41,42]. Additionally, the morphologies, including sizes, aspect ratios,

and shapes, of nanofillers directly affect how easily the percolation network can be formed. 1D nanomaterials with high aspect ratios, such as carbon nanotubes (CNTs)[43] and metallic nanowires[34,44], are suitable for achieving highly conductive nanocomposites with minimal filler amounts due to their relatively low percolation thresholds.

This chapter provides an overview of widely-used conductive nanofillers and their impact on the electrical and mechanical properties of nanocomposites. We describe the unique features and the advantages and disadvantages of these composites, which depend on the material types and morphologies of the nanofillers (see Table 1 for a summary). The chapter also provides general guidelines for selecting materials for high-performance stretchable conductive nanocomposites, including strategies for modifying fillers and fabrication methodologies.

Soft conductive nanocomposites based on carbon nanofillers

Carbon-based nanofillers, such as carbon black (CB)[45-47], graphene[48-51], and CNTs[52-54], have unique features that make them suitable for use in conductive nanocomposites. These materials possess high electrical conductivity due to the transfer of electrons via delocalized π-orbitals, which enables the fabrication of high-performance nanocomposites[55,56]. Furthermore, carbon-based nanomaterials are known for their excellent mechanical properties[57-59], low production costs[60], and ease of functionalization[61,62]. In this section, we introduce stretchable conductive nanocomposites based on carbon-based nanofillers.

CB particles are spherical particles whose diameters range from 10 to 100 nm. CB has been used as a filler for rubbers to enhance tensile strength and/or abrasion resistance[63]. Owing to its electrical conductivity, elastomers mixed with CB at concentrations of 10% or higher can become electrically conductive. For instance, Niu *et al.* synthesized a nanocomposite of CB and polydimethylsiloxane (PDMS) by simply mixing the CB powder with PDMS[45]. The cross-sectional scanning electron microscopy (SEM) image of the resulting nanocomposite showed that the CB particles were uniformly distributed and connected with each other inside PDMS [Figure 2A, left]. The nanocomposite exhibited electrical conductivity of ~25 $S \cdot m^{-1}$ and a percolation threshold of ~10 wt%. The strain-dependent electrical conductivity change was also measured, and the electrical conductivity increased monotonically as the applied strain increased, especially at the low strain regime [Figure 2A, right]. By using a soft lithography technique, planar and 3D microstructures of the nanocomposite could be fabricated, proving its potential for application to microelectronic devices. However, owing to the 0D structure and the low aspect ratio of CB that lead to a relatively high percolation threshold and the low electrical conductivity of the CB-based nanocomposites, its application to high-performance electronics has been limited.

Graphene and its derivatives, such as graphene oxide (GO) and graphite, have been highlighted as another type of carbon-based filler for their higher electrical and mechanical performances than CB. Graphene is an allotrope of carbon in which sp^2 hybridized atoms are arranged as a single layer with a 2D honeycomb structure. Hence, graphene can achieve a low percolation threshold and exhibit transparency[64-66]. An interesting example is the 3D foam-like graphene macrostructure (graphene foam). Chen *et al.* synthesized the graphene foam upon a 3D interconnected porous nickel foam by using chemical vapor deposition [Figure 2B, left][48]. Due to its high charge carrier mobility arising from the unique interconnect network, a graphene foam/PDMS composite showed relatively high electrical conductivity of ~10 $S \cdot cm^{-1}$, even at an ultralow graphene content of ~0.5 wt% [Figure 2B, right]. Moreover, infiltrating the graphene foam with the polymer matrix improved mechanical properties of the composite. As a result, the resistance of graphene foam/PDMS composite increased by only ~30% under ~50% strain. In another research conducted by Liu *et al.*, highly stretchable and transparent graphene electrodes could be fabricated by intercalating graphene

Table 1. Comparison of soft conductive nanocomposites with different types of filler materials

Classification	Advantages	Disadvantages	Filler	Matrix	Optimal filler content	Conductivity	Stretchability	Change in electrical properties under strain	Ref.
Carbon-based nanomaterials	Low production cost; Mechanical robustness; Ease of functionalization	Low conductivity	CB	PDMS	26 wt%	0.25 $S \cdot cm^{-1}$	50%	0.29 $S \cdot cm^{-1}$ at 50% strain	[45]
			CB	SBS	11.1 vol%	0.15 $S \cdot cm^{-1}$	300%	0.07 $S \cdot cm^{-1}$ at 300% strain	[46]
			CB	PDMS	15 wt%	_	80%	$\Delta R/R_0$ = 50% at 10% strain, $\Delta R/R_0$ = 150% at 80% strain	[47]
			Graphene	PDMS	0.5 wt%	10 $S \cdot cm^{-1}$	90%	$\Delta R/R_0$ = 30% at 50% strain	[48]
			Graphene	SEBS	-	100 $\Omega \cdot sq^{-1}$	120%	$\Delta R/R_0$ = 50% at 100% strain	[67]
			GO	PDMS	0.83 vol%	1,660 $\Omega \cdot cm$	40%	$\Delta R/R_0$ = 950% at 40% strain	[68]
			GO	PDMS	40 wt%	0.27 $S \cdot cm^{-1}$	60%	$\Delta R/R_0$ = 170% at 60% strain	[69]
			Graphite	PU	83.3 wt%	0.50 $S \cdot cm^{-1}$	100%	$\Delta R/R_0$ = 25% at 30% strain	[70]
			CNT	PDMS	-	6 $\Omega \cdot sq^{-1}$	100%	$\Delta R/R_0$ = 50% at 100% strain	[43]
			SWCNT	PDMS	5.1 wt%	30 $S \cdot cm^{-1}$	60%	Stable conductivity within 60% strain	[52]
			SWCNT	PDMS	20 wt%	57 $S \cdot cm^{-1}$	110%	Stable conductance within 50% strain	[72]
			Graphene/CNT	Alginate	0.1 wt%/1.2 wt%	0.35 $S \cdot cm^{-1}$	50%	Stable impedance after 10,000 cycles of 11% biaxial strain	[59]
Conducting polymer	Easy processability; Tunable electrochemical properties; Reasonable conductivity	Low intrinsic stretchability	PEDOT:PSS	SEBS	-	2,700 $S \cdot cm^{-1}$	150%	6,000 $S \cdot cm^{-1}$ at 100% strain	[87]
			PEDOT:PSS	PVA	7.1 wt%	10 $S \cdot cm^{-1}$	600%	-	[83]
			PEDOT:PSS	PAAc	1.1 wt%	23.7 $S \cdot cm^{-1}$	163%	$\Delta R/R_0$ = 10% at 100% strain	[85]
			PANI	SEBS	15 vol%	200 $S \cdot cm^{-1}$	180%	Stable conductivity within 60% strain	[170]
			PPy	PCTC	-	116 $S \cdot cm^{-1}$	25%	$\Delta R/R_0$ = 15% at 20% strain	[203]
			PPy	PU	-	238 $S \cdot cm^{-1}$	900%	5,300 $S \cdot cm^{-1}$ at 800% strain	[204]
			P3BT	TFB	50 wt%	4 $S \cdot cm^{-1}$	2,000%	Stable conductivity within 2,000% strain	[205]
Metal-based nanomaterials	High conductivity	Biocompatibility	AgNP	PEG	67 wt%	21,000 $S \cdot cm^{-1}$	70%	Stable conductivity within 50% strain	[98]
			AgNP	PVDF-HFP	8.5 wt%	2,680 $S \cdot cm^{-1}$	350%	100 $S \cdot cm^{-1}$ at 50% strain	[99]
			AuNP	PU	16.2 vol%	11,000 $S \cdot cm^{-1}$	110%	3,500 $S \cdot cm^{-1}$ at 60% strain	[97]
			AgNW	SBS	18 vol%	10,500 $S \cdot cm^{-1}$	100%	$\Delta R/R_0$ = 20% at 100% strain	[93]
			AgNW	PUA	6.6 wt%	46,700 $S \cdot cm^{-1}$	80%	10,000 $S \cdot cm^{-1}$ at 70% strain	[100]

			AgNW	PU	-	9,100 S·cm^{-1}	310%	$\Delta R/R_0$ = 45% at 50% strain	[101]
			AgNW	SEBS	-	> 100,000 S·cm^{-1}	540%	$\Delta R/R_0$ = 1,000% at 150% strain	[44]
			Ag-AuNW	SBS	60 wt%	41,850 S·cm^{-1}	266%	10,000 S·cm^{-1} at 100% strain	[107]
			Ag-Au-PtNW	SEBS	60 wt%	11,000 S·cm^{-1}	480%	$\Delta R/R_0$ < 1,000% at 200% strain	[37]
			AuNS	TPU	7.9 vol%	1,600 S·cm^{-1}	200%	$\Delta R/R_0$ = 800% at 200% strain	[106]
			AgNP/AgNW	SEBS	40 wt%/40 wt%	31,000 S·cm^{-1}	800%	$\Delta R/R_0$ = 0.26% at 50% strain	[34]
Liquid metals	Strain insensitivity; Theoretically infinite stretchability; Metal-like intrinsic conductivity	Biocompatibility; Need for encapsulation	EGaIn	PDMS	-	960 S·cm^{-1}	-	-	[126]
			EGaIn	PDMS	50 vol%	1,370 S·cm^{-1}	-	$\Delta R/R_0$ < 10% at 50% strain	[131]
			EGaIn	PDMS/VHB	-	20,600 S·cm^{-1}	1,200%	$\Delta R/R_0$ = 6% at 100% strain	[133]
			EGaIn	SBS	-	100 S·cm^{-1}	1,800%	$\Delta R/R_0$ = 40% at 1,800% strain	[137]
			EGaIn	PEGDA	10 vol%	5 Ω·sq^{-1}	17%	-	[138]

Ag-AuNW: silver-gold core-shell nanowire; Ag-Au-PtNW: silver-gold-platinum core-shell-shell nanowire; AgNP: silver nanoparticle; AgNW: silver nanowire; AuNP: gold nanoparticle; AuNS: gold nanosheet; CB: carbon black; CNT: carbon nanotube; EGaIn: eutectic gallium-indium; GO: graphene oxide; PAAc: poly(acrylic acid); PANI: polyaniline; PCTC: polycaprolactone-b-polytetrahydrofuran-b-polycaprolactone; PDMS: polydimethylsiloxane; PEDOT:PSS: poly(3,4-ethylenedioxythiophene):poly(styrene sulfonate); PEG: poly(ethylene glycol); PEGDA: poly(ethylene glycol) diacrylate; PPy: polypyrrole; PU: polyurethane; PUA: poly(urethane acrylate); PVA: poly(vinyl alcohol); PVDF-HFP: poly(vinylidene fluoride-co-hexafluoropropylene); P3BT: poly(3-butylthiophene-2,5-diyl); SBS: poly(styrene-butadiene-styrene); SEBS: poly[styrene-b-(ethylene-co-butylene)-b-styrene]; SWCNT: single-walled carbon nanotube; TFB: poly[(9,9-dioctylfluorenyl-2,7-diyl)-co-(4,4′-(N-(4-sec-butylphenyl)diphenylamine)]; TPU: thermoplastic polyurethane.

nanoscrolls between graphene layers[67]. The multilayer graphene/graphene scrolls exhibited a sheet resistance of ~100 Ω·sq^{-1} with a transparency of ~90%. Since some scrolls bridged the cracked regions of graphene under external strain, the resistance of multilayer graphene/graphene scrolls supported on poly[styrene-b-(ethylene-co-butylene)-b-styrene] (SEBS) substrates increased by only ~50% under ~100% strain.

GO is a chemically modified derivative of graphene with oxygen-containing functional groups. Due to the hydrophilic functional groups, GO can be dispersed in polar solvents, which makes the fabrication process of GO-based devices easier[68,69]. Shi *et al.* developed a nanocomposite ink composed of water-soluble PDMS submicrobeads and GO[68]. The water-soluble PDMS submicrobeads were obtained by dissolving the prepolymer of PDMS in dichloromethane (DCM), mixing them with poly(vinyl alcohol) (PVA) aqueous solution to form an emulsion, and evaporating DCM. Next, the PDMS submicrobeads and GO were mixed in water to fabricate a GO/PDMS nanocomposite ink [Figure 2C, left]. The nanocomposite ink could be used to make desired patterns by using 3D

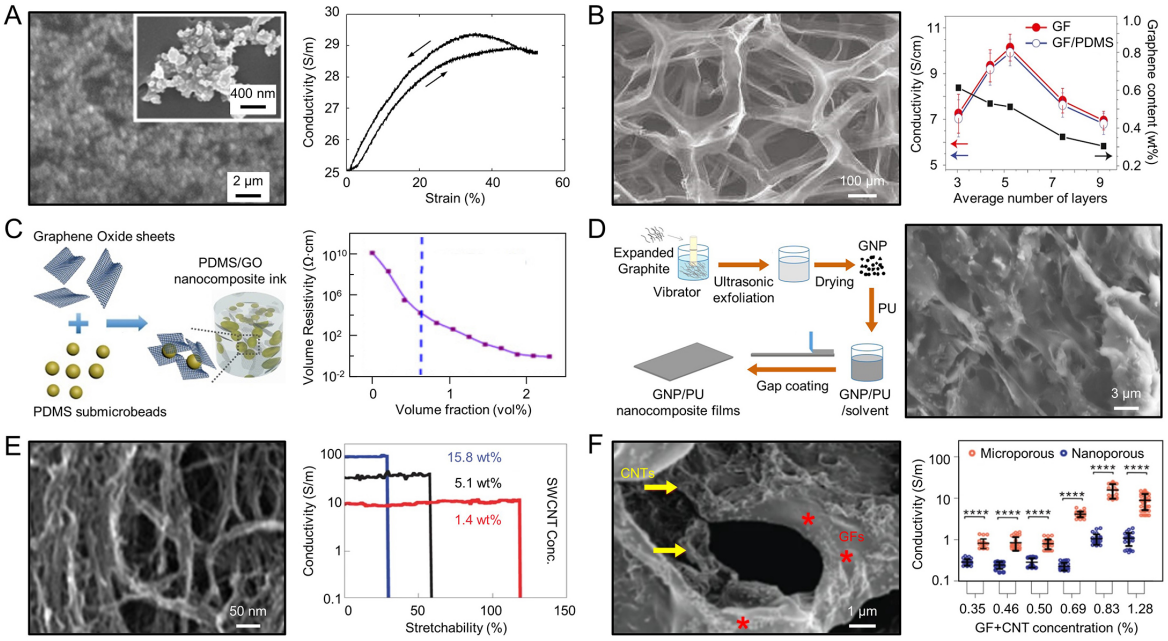

Figure 2. Soft conductive nanocomposites based on carbon nanofillers. (A) SEM image of CB powder (left) and the conductivity variation of a CB-PDMS composite under stretching (right). Reproduced with permission from ref[45]. Copyright 2007, WILEY-VCH Verlag GmbH & Co. KGaA, Weinheim; (B) SEM image of graphene foam (GF) (left) and the conductivity of GF and GF/PDMS composites with respect to the number of graphene layers (right). Reproduced with permission from ref[48]. Copyright 2011, Nature Publishing Group; (C) Schematic illustration of the fabrication of PDMS submicrobead/GO nanocomposite ink (left) and the volume resistivity as a function of GO volume fraction. Reproduced with permission from ref[68]. Copyright 2019, Elsevier Ltd; (D) Schematic illustration of the fabrication process of GNP/PU nanocomposite films (left) and cross-sectional SEM image of the film (right). Reproduced with permission from ref[70]. Copyright 2017, American Chemical Society; (E) SEM image of SWCNTs uniformly dispersed in rubber (left) and the conductivity of printed elastic conductor as a function of stretchability with different concentrations of SWCNT (right). Reproduced with permission from ref[52]. Copyright 2009, Nature Publishing Group; (F) SEM image of a conductive alginate hydrogel with GFs and CNTs (left). Red asterisks indicate regions containing GFs, and yellow arrows point to CNTs. The conductivity of microporous and nanoporous hydrogels with increasing concentrations of carbon fillers (right). Reproduced with permission from ref[59]. Copyright 2021, The Author(s), under exclusive license to Springer Nature Limited. CB: Carbon black; CNTs: carbon nanotubes; GFs: graphene flakes; GO: graphene oxide; GNP: graphene nanoplate; PDMS: polydimethylsiloxane; PU: polyurethane; SEM: scanning electron microscopy; SWCNT: single-walled carbon nanotube.

printing and thermal annealing. The nanocomposite exhibited a resistivity of 1,660 Ω·cm with a low percolation threshold of 0.83 vol% owing to the unique network structure of the graphene-wrapped PDMS beads [Figure 2C, right].

Graphite is a stacked form of 2D graphene sheets, which is one of natural carbon nanomaterials. Although forming a highly percolated network with graphite is more challenging than with graphene, graphite has the advantage of a facile preparation process, thus allowing low production cost and potential for industry-level mass production[70,71]. For example, Wu *et al.* produced nanocomposite films composed of graphite nanoplates (GNPs) and polyurethane (PU)[70]. Initially, expanded graphite particles were fragmented and exfoliated by ultrasonication to prepare GNPs. After homogenously mixing GNPs with PU in an organic solvent, the GNP/PU nanocomposite film was fabricated by a gap coating method with the solution [Figure 2D, left]. The GNP/PU nanocomposite film, in which GNPs are well distributed in the elastomeric matrix without the exposure of sharp edges of GNPs, exhibited appropriate flexibility and electrical conductivity of ~50 $S \cdot m^{-1}$ [Figure 2D, right]. Moreover, nanocomposite films with a length of ~3 m and a width of 0.3 m could be manufactured, demonstrating its potential for industrial mass production.

Among conductive carbon-based nanomaterials, CNTs are considered one of the most suitable fillers to form a percolation network owing to their high aspect ratios[43,72]. For instance, Sekitani *et al.* developed printable elastic conductors with single-walled CNTs (SWCNTs) dispersed in a fluorinated copolymer matrix[52]. A jet-milling process enabled a uniform dispersion of fine SWCNTs without shortening their length [Figure 2E, left], whereas typical dispersing methods, such as ultrasonication, grinder-milling, and ball-milling, made SWCNT bundles finer but shorter, which reduced the electrical conductivity of their percolated network. The conductive ink prepared by mixing SWCNTs, an ionic liquid, and a fluorinated copolymer was screen-printed and dried on a PDMS substrate. The printed elastic conductors exhibited the maximum conductivity of 102 $S \cdot cm^{-1}$ (at 15.8 wt% of SWCNTs) and the maximum stretchability of 118% (at 1.4 wt% SWCNTs) [Figure 2E, right]. Taking advantage of their excellent electrical conductivity, stretchability, and processability, an active-matrix display was successfully fabricated with the elastic conductor. Due to its stretchability, the display could be conformally mounted on a hemispherical surface.

Further improvement in the material performance could be made by integrating multiple carbon-based nanofillers. For example, Tringides *et al.* fabricated a conductive alginate hydrogel loaded with graphene flakes (GFs) and CNTs[59]. The hydrogel was modified to possess micropores by lyophilization before crosslinking. GFs were connected to CNT bundles dispersed in the porous matrix, improving the probability of forming a percolation network [Figure 2F, left]. Hence, the highly porous alginate hydrogel retained an ultrasoft modulus and improved electrical conductivity. The carbon-based hydrogel exhibited a conductivity of 35 $S \cdot m^{-1}$ and a percolation threshold of ~0.9 wt% carbon [Figure 2F, right]. In addition, the charge storage capacity (CSC) of the hydrogel could be tuned by varying the relative ratio of GFs and CNTs, which suggested the possibility for further optimization of sensing and/or stimulation performance. Viscoelastic electrode arrays that have tissue-like mechanical properties were fabricated and exhibited excellent long-term electrical stability even after 10,000 cycles of 11% biaxial strain.

As introduced above, carbon nanofillers have shown potential for use in soft wearable bioelectrodes. However, concerns arise regarding their biocompatibility and cytotoxicity when in contact with living organisms. Possibilities for the skin irritation, inflammation, oxidative stress, and even cancer have been reported for chronic use of CB[73,74], graphene[75], and CNTs[76]. The cytotoxicity of these materials is related to the factors such as sizes, concentrations, and surface modifications. To address these concerns, researchers have been actively exploring surface modification methods, encapsulation techniques, and handling protocols to enhance biocompatibility and minimize cytotoxic effects. Regulatory guidelines also play a crucial role in ensuring the safe use of these materials in soft wearable electronics.

Carbon-based nanocomposites offer several benefits, such as mechanical robustness, chemical stability, and easy mass production. However, their intrinsic conductivities are lower than those of metal-based nanocomposites, which can limit their use in certain device applications. To overcome this limitation, researchers are exploring various material strategies to improve the electrical and electromechanical properties of carbon-based nanocomposites.

Soft conductive composites based on conducting polymers

CPs have become increasingly popular as filler materials for stretchable conductors, particularly for bioelectronics applications[77-79]. This is due to their attractive features, such as reasonable conductivity[80], mechanical ductility[81], tunable electrochemical properties[82], and easy processability[83,84]. CPs have fibril structures and single polymer dimensions similar to nanomaterials. In this section, we introduce some representative stretchable conductors that use CPs, such as poly(3,4-ethylenedioxythiophene):poly(styrene sulfonate) (PEDOT:PSS), polyaniline (PANI), and polypyrrole (PPy).

PEDOT:PSS is the most researched CP due to its electrical and mechanical performance[85,86]. Jiang *et al.* designed a modified version of PEDOT:PSS to achieve high conductivity, stretchability, and photopatternability by introducing a topological supramolecular network[87]. A supramolecular additive with a polyrotaxane structure composed of a polyethylene glycol (PEG) backbone and cyclodextrins (CDs) side chains was blended into PEDOT:PSS [Figure 3A, left]. The PEG backbone induced aggregation of PEDOT, which improved electrical conductivity. The CDs improved mobility along the direction of the polymer chain, enhancing stretchability. Consequently, PEDOT:PSS blended with the supramolecular additive exhibited two orders of magnitude higher conductivity [Figure 3A, right] and could be stretched up to over 100% without cracking. A stretchable electrode array could be fabricated, which was conformally attached to human skin to capture EMG signals.

In another example, Tan *et al.* prepared a self-adhesive conductive polymer (SACP) composite based on PEDOT:PSS[83]. The SACP was fabricated by homogeneously mixing an elastic polymer (PVA crosslinked with glutaraldehyde) and a supramolecular solvent (citric acid and CD) with an aqueous solution of PEDOT:PSS [Figure 3B, left top]. Strong interfacial adhesion of the SACP arose from multiple interactions, including hydrogen bonds, ionic interactions, and Van der Waals interactions [Figure 3B, left bottom]. The SACP could be prepared as a conductive film by spin-coating or drop-casting. The SACP film exhibited conductivities ranging from 1 to 37 $S \cdot cm^{-1}$. Also, the SACP film could be conformally attached to the skin, thereby offering conductive human-device interfaces [Figure 3B, right].

Rapid solidification of CPs in solvents was a major obstacle to fabricating CP fibers using wet spinning techniques[88]. Fang *et al.* reported wet-spun, ultrafine PANI fibers by adopting a solvent exchange strategy [Figure 3C, left][84]. Generally, PANI was doped with camphor sulfonic acid in cresol for conductivity[89]. However, doped PANI was incompatible with conventional wet spinning protocols due to its rapid solidification into thick gels, which is induced by strong interactions between doped CPs. By replacing cresol with dimethyl formamide (DMF), however, PANI could be well dispersed. PANI gel protofibers with a low viscosity below 3,000 cP could be obtained, and subsequently, PANI fibers with a diameter below 5 μm were drawn. Ultrafine PANI fibers with maximized electroactive surfaces exhibited superb CSCs and unprecedented mechanical strength of 1,080 MPa [Figure 3C, right].

Further conductivity enhancement was achieved by synthesizing 1D nanostructured CP hydrogel, as demonstrated by Wang *et al.*[90]. They developed a PPy hydrogel with nanofiber-like structures using a disc-shaped dopant, copper phthalocyanine-3,4′,4″,4‴-tetrasulfonic acid tetrasodium salt (CuPcTs). Steric and electrostatic interactions between CuPcTs and PPy induced in situ self-assembly of PPy, resulting in 1D growth of PPy chains [Figure 3D, left]. The 1D morphology and porous structure promoted the transfer of electrons and ions, which improved the electrochemical property and electrical conductivity. The PPy-CuPcTs hydrogel exhibited lower impedance and two orders of magnitude higher conductivity (7.8 $S \cdot cm^{-1}$) than pristine PPy [Figure 3D, right]. Moreover, considering that the water content of the hydrogel was as high as 94 wt%, CP hydrogels showed great potential as biosensors owing to their excellent solution processability and high permeability to ions and molecules.

The use of conductive polymers may raise several concerns regarding their biocompatibility. These include the potential cytotoxicity of the polymers and their degradation byproducts, the risk of allergic reactions in some individuals, the long-term stability of the polymers and their impact on biocompatibility over extended periods, the mechanical compatibility of the materials with the skin to avoid discomfort or injury, and the influence of surface characteristics on interactions with the skin, such as bacterial adhesion or tissue irritation[91,92]. Addressing these concerns requires a multidisciplinary approach involving material design,

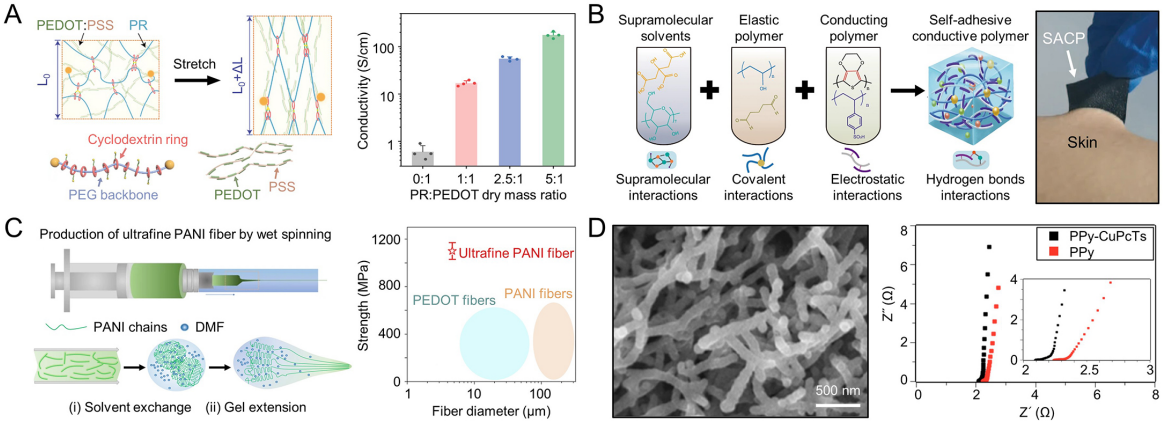

Figure 3. Soft conductive composites based on conducting polymers. (A) Schematic illustration of the topological supramolecular network with a polyrotaxane (PR)-structure supramolecular additive and PEDOT:PSS (left). The conductivity of the polymer film with increasing PR content (right). Reproduced with permission from ref[87].Copyright 2022, The American Association for the Advancement of Science; (B) Schematic illustration of the fabrication and interactions of the SACP (left) and an image depicting the adhesion of the SACP film on the skin of the arm (right). Reproduced with permission from ref[83].Copyright 2022, The Author(s); (C) Schematic illustration of the solvent exchange strategy to produce the ultrafine PANI fiber in a modified wet spinning protocol (left). Ashby plot comparing the mechanical strength of the ultrafine PANI fiber to previously reported conducting polymer fibers. Reproduced with permission from ref[84].Copyright 2022, The Author(s); (D) SEM image of the nanostructured PPy-CuPcTs hydrogel (left). Electrochemical impedance plot of PPy-CuPcTs hydrogel compared with pristine PPy (right) and zoom in of the plot (right inset). Reproduced with permission from ref[90].Copyright 2015, American Chemical Society. CuPcTs: copper phthalocyanine-3,4′,4″,4‴-tetrasulfonic acid tetrasodium salt; DMF: dimethyl formamide; PANI: polyaniline; PEDOT:PSS: poly(3,4-ethylenedioxythiophene):poly(styrene sulfonate); PEG: polyethylene glycol; PPy: polypyrrole; SACP: self-adhesive conductive polymer.

surface modifications, and comprehensive biocompatibility testing while adhering to regulatory standards to ensure the safe integration of conductive polymers into soft wearable electronics.

The structural diversity and synthetic tunability of CPs enable molecular engineering, such as doping and forming supramolecular networks. Therefore, CP-based composites are able to exhibit higher conductivities than carbon-based nanocomposites and present new functionalities, such as micropatternability, self-adhesion, and solution processibility. They also satisfy material requirements for bioelectronics, such as superior electrochemical properties and biocompatibility. However, conductivities are still much lower than those of metal-based nanocomposites. Further studies for material development are required to achieve advanced devices using CP-based composites.

Soft conductive nanocomposites based on metal nanofillers

Metal nanofillers are one of the most studied types of fillers, as they exhibit high intrinsic conductivity (up to 6×10^5 S·cm^{-1})[93]. Moreover, since metal nanofillers can be fabricated into desirable sizes, structures, and dimensions, they provide versatile features to the nanocomposites[94-96]. In this section, soft and conductive nanocomposites based on various metal nanofillers are described, with details on how each form of nanofiller affects the overall performance of the nanocomposites.

Among the different dimensions of metal nanomaterials, 0D nanoparticles are the most basic form that can be rather easily synthesized with various metal elements[97]. Numerous studies have been conducted on fabricating nanocomposites with nanoparticles, especially with silver nanoparticles (AgNPs) that can be readily synthesized and exhibit high intrinsic conductivity (6.3×10^5 S·cm^{-1}). For instance, Hyun *et al.* fabricated a nanocomposite of AgNPs and PEG in an ordered zigzag morphology [Figure 4A, left][98]. The

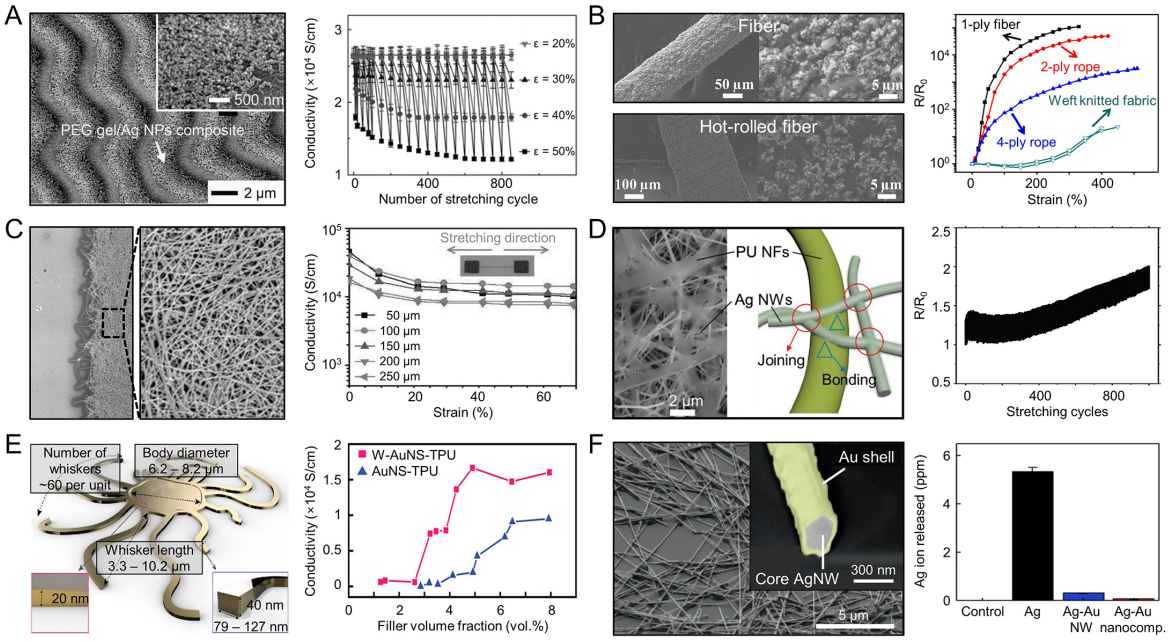

Figure 4. Soft conductive nanocomposites based on metal nanofillers. (A) SEM images of the composite in a zigzag morphology (left) and electrical conductivity changes under repeated stretching (right). Reproduced with permission from ref[98]. Copyright 2011, WILEY-VCH Verlag GmbH & Co. KGaA, Weinheim; (B) Schematic of the wet spinning apparatus and image of a knitted fabric (left). Normalized resistance change as a function of tensile strain (right). Reproduced with permission from ref[99]. Copyright 2014, American Chemical Society; (C) Schematic of screen printing of a water-based AgNW ink and optical image of AgNW patterns (left). Conductivity variation of the conductive ink-based composite under stretching (right). Reproduced with permission from ref[100]. Copyright 2016, WILEY-VCH Verlag GmbH & Co. KGaA, Weinheim; (D) SEM image (left) and schematic of nanomesh conductor (middle). Resistance change under repeated stretching at 50% tensile strain (right). Reproduced with permission from ref[101]. Copyright 2019, WILEY-VCH Verlag GmbH & Co. KGaA, Weinheim; (E) Schematic of W-AuNS (left) and the conductivity against filler volume fraction (right). Reproduced with permission from ref[106]. Copyright 2022, American Chemical Society; (F) SEM image and backscattered electron (BSE) image of Ag-Au core-sheath nanowire (left) and ICP-MS analysis on Ag ions released (right). Reproduced with permission from ref[107]. Copyright 2018, The Author(s). AgNPs: silver nanoparticles; AgNW: silver nanowire; ICP-MS: inductively coupled plasma-mass spectrometry; PEG: polyethylene glycol; PU: polyurethane; SEM: scanning electron microscopy; TPU: thermoplastic polyurethane; W-AuNS: whiskered gold nanosheet.

nanocomposite was fabricated by gelating PEG with AgNPs in the valley of the buckled surface of the manufactured template using PDMS and polystyrene. Micrometer-scale patterning could be achieved by placing AgNPs in a desired part rather than randomly dispersing them in the gel. It exhibited a conductivity of 2.1×10^4 S·cm^{-1} with 67 wt% AgNPs and high mechanical durability (700 stretching cycles of 50% strain) [Figure 4A, right]. A stretchable electrode was fabricated by double transfer of the zigzag composites in a perpendicular configuration, which also showed 70% transparency in the visible region.

AgNP-based nanocomposites in the form of stretchable fiber have also been reported. For example, Ma *et al.* developed a fiber with a diameter of ~17 μm using a wet spinning and hot rolling process[99]. They injected a mixture of AgNPs with a size range of 100-150 nm, multi-walled CNTs (MWCNTs) decorated with AgNPs ranging in size from 3 to 5 nm, and poly(vinylidene fluoride-co-hexafluoropropylene) (PVDF-HFP). The mixture was extracted in hexane and hot-roll-pressed to obtain a more uniform distribution of fillers and increase the filler density of the fiber [Figure 4B, left]. The resulting fiber exhibited an initial conductivity of ~17,460 S·cm^{-1} with a maximum tensile strain of 50%. It could be twisted and woven into a weft-knitted fabric and showed stable conductivity up to ~200% strain [Figure 4B, right]. However, there is room to further increase conductivity, considering the low aspect ratio of nanoparticles.

1D nanowires have a higher aspect ratio than 0D nanoparticles and thus can achieve a highly percolated network and higher conductivity[34]. Among metallic nanowires, silver nanowires (AgNWs) have been widely used because very long AgNWs can be synthesized in large quantities. For example, Liang *et al.* fabricated a highly conductive and stretchable nanocomposite using a water-based AgNW ink with ~50 μm pattern resolution [Figure 4C, left][100]. The AgNW-based conductive ink exhibited a high conductivity of 4.67×10^4 S·cm^{-1} with only 10.4 wt% AgNWs and still maintained a conductivity higher than 10,000 S·cm^{-1}, even at 70% tensile strain [Figure 4C, right]. It outperformed AgNP-based conductive inks, whose conductivity was 5,710 S·cm^{-1} at 0% strain and 20 S·cm^{-1} at 140% strain.

AgNW-based nanocomposites have demonstrated high initial conductivity and outstanding electrical stability under strain, but they often lack cyclic durability due to their fragile nature under repetitive stress. Therefore, Jiang *et al.* proposed new porous nanomesh-type elastomeric conductors to mitigate this durability issue [Figure 4D, left][101]. By forming hydrogen bonds between poly(vinylpyrrolidone) (PVP) ligands grafted on the AgNW surface and PU nanofibers, a nanocomposite with a layer-by-layer structure was fabricated. The porosity of the nanocomposite imparted permeability and was attributed to low flexural rigidity. The nanocomposite exhibited both high conductivity of 9,100 S·cm^{-1} and a high stretchability of 310%. The resistance increased only by 75% after 1,000 stretching cycles of 50% strain [Figure 4D, right].

Although AgNWs are frequently utilized for fabricating highly conductive and stretchable nanocomposites, they lack biocompatibility to be used for in vivo applications due to their cytotoxicity caused by leaching silver ions[102]. In order to suppress such shortcomings, research has been conducted to develop gold-based biocompatible nanofillers[103-105]. However, since the typical diameter of AuNWs is less than 30 nm, it is difficult to achieve the same level of conductivity as AgNW-based nanocomposites. Instead of AuNWs, Lim *et al.* developed a novel 2D material, whiskered gold nanosheets (W-AuNSs), for conductive, stretchable, and biocompatible nanocomposites [Figure 4E, left][106]. Due to its unique structure with long ribbon-shaped whiskers, the W-AuNS formed a percolation network at 1.56 vol%, much lower than that of AuNP (5.02 vol%) and AuNS (2.74 vol%). When fabricated into a nanocomposite with thermoplastic PU (TPU), it exhibited a conductivity of 1,600 S·cm^{-1} [Figure 4E, right] and a stretchability of 200%.

In addition to the synthesis of pure gold nanofillers, wrapping a gold (Au) shell on silver nanomaterials presents a promising strategy to achieve biocompatibility. For example, Choi *et al.* developed ultralong Ag-Au core-sheath nanowires by coating an Au shell on AgNW and applied them to implantable devices [Figure 4F, left][107]. The Ag-Au core-sheath nanowire had the advantages of both the high aspect ratio of AgNWs and the biocompatibility of Au [Figure 4F, right]. By dispersing the Ag-Au nanowire in poly(styrene-butadiene-styrene) (SBS), a nanocomposite with high conductivity (41,850 S·cm^{-1}) and high stretchability (266%) could be fabricated.

Recently, Sunwoo *et al.* fabricated a biocompatible, low-impedance nanocomposite comprising Ag-Au-platinum (Pt) core-shell-shell nanowires and Pt nanoparticles dispersed in SEBS[37]. Additional Pt shells in the Ag-Au-Pt nanowires effectively reduced Ag ion leaching by 99%, leading to significantly improved cell viability compared to Ag-Au nanowires. The embossed surface morphologies of the Ag-Au-Pt nanowires, along with the *in situ* synthesized Pt nanoparticles, increased the effective surface area and reduced contact impedance while maintaining high conductivity (11,000 S·cm^{-1}) and excellent stretchability (480%).

As briefly discussed above, metallic nanomaterials, such as silver nanomaterials[108,109], metal oxides[110], and even gold nanomaterials[111,112], may exhibit cytotoxic effects depending on factors such as sizes, shapes,

surface chemistry, and concentrations. These nanomaterials can potentially induce oxidative stress, inflammation, and cellular damage. Long-term exposure or systemic absorption of metallic nanoparticles can lead to adverse health effects. Additionally, the release of metallic ions from nanomaterials may pose toxicity risks. Ensuring the biocompatibility of metallic nanomaterials in soft wearable electronics requires careful consideration of material selection, surface modifications, and thorough biocompatibility assessments to minimize potential risks to users.

With the development of facile metal nanomaterial fabrication, extensive research has been conducted on nanocomposites with various nanofillers of different dimensions. These metal-based nanocomposites can enhance both electrical and mechanical properties of materials. While AgNW-based nanocomposites have performed exceptionally well, recent studies have focused on materials other than silver to improve biocompatibility.

Soft conductive nanocomposites based on liquid metals

LMs are unique metals and metal alloys that remain in a liquid state near room temperature due to their low melting points[113]. The combination of metallic and liquid properties, such as high thermal and electrical conductivities[114], low viscosities[115], and excellent deformability[116], makes them highly versatile and valuable in many applications[117-120]. Ga-based alloys, including eutectic Ga-In (EGaIn) and Ga-In-Sn (Galinstan), have been most widely used due to their low toxicity and high chemical stability compared to other LM counterparts[121], such as Hg (which is toxic)[122] and Cs (which is explosively reactive)[123].

In recent years, researchers have synthesized various LM-based composites in which LMs are dispersed in an elastomeric matrix as micro- or nanodroplets[124]. These efforts were focused on utilizing the high intrinsic conductivity of LMs while preserving the mechanical properties of the elastomer matrix. However, typical LM-based composites are inherently nonconductive due to the thin oxide layer on the surface of LM droplets[125]. Therefore, an additional process (e.g., mechanical sintering[126,127], laser sintering[128,129], or thermal expansion[130]) should be introduced to create electrical pathways by rupturing the oxide layer and coalescing adjacent LM droplets. For instance, Lin *et al.* embedded EGaIn nanoparticles in PDMS sheets and created conductive traces by mechanical sintering[126]. The EGaIn nanoparticles with an average diameter of ~105 nm were prepared by sonicating bulk EGaIn in ethanol [Figure 5A, left] and cast on top of the PDMS film. After solvent evaporation, a PDMS prepolymer was poured onto the EGaIn-PDMS film and cured to form a PDMS-EGaIn-PDMS structure. Then, external pressure was locally applied to merge EGaIn nanoparticles together [Figure 5A, right]. To demonstrate the concept, they measured the current-voltage curves before and after mechanical sintering. The electrical conductivity increased by a factor of 4×10^8 after sintering, exhibiting 960 $S \cdot cm^{-1}$.

Laser sintering has emerged as another facile process for fabricating conductive LM-based composites. Liu *et al.* created conductive EGaIn nanoparticle films on various substrates via laser sintering and investigated their electrical properties depending on laser fluence, nanoparticle size, substrate material, and film thickness[128]. The spray-printed EGaIn nanoparticles were treated by a pulsed laser with a wavelength of 1,065 nm. The oxide layer on the surface of the EGaIn particle was transparent to light with wavelengths greater than 300 nm, while the gallium-indium core was heated by a photothermal effect. Therefore, the oxide layer was ruptured due to thermal expansion of the heated EGaIn core, allowing EGaIn nanoparticles to flow and form conductive networks [Figure 5B, left]. Among various processing parameters, the laser fluence (energy per unit area) was the most important factor that determined the resistance of the EGaIn film, while the particle size and film thickness had negligible effects. As more energy was transferred during sintering, more particles coalesced with neighboring particles, resulting in a decrease in resistance [Figure 5B, right].

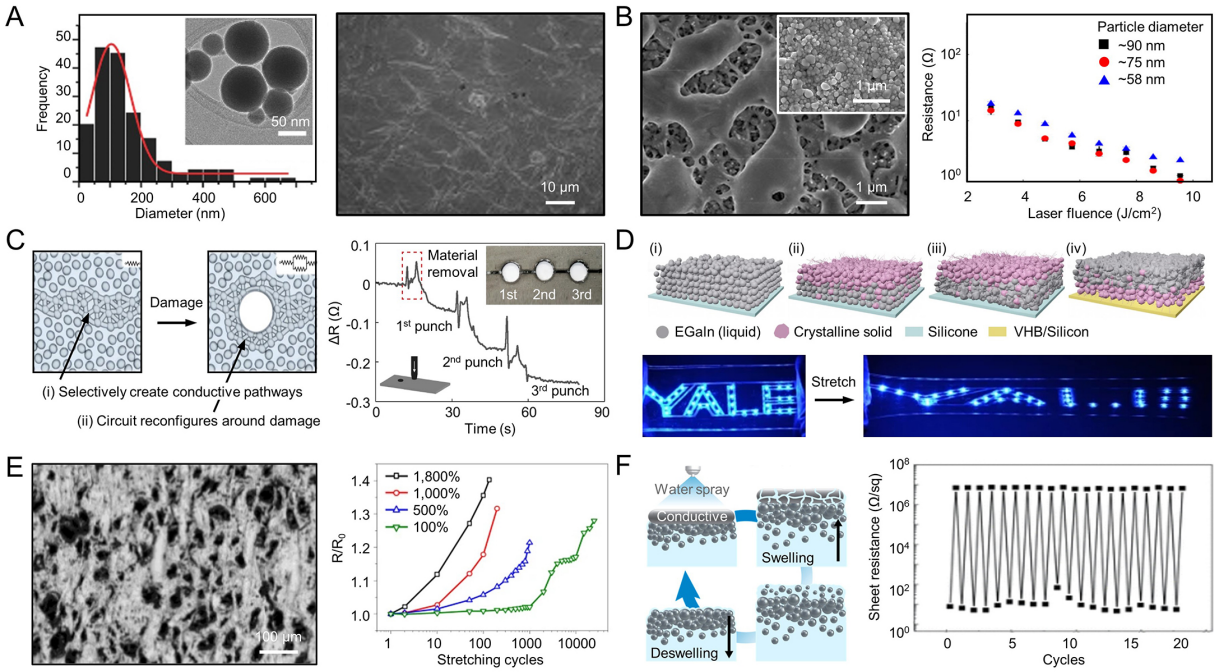

Figure 5. Soft conductive nanocomposites based on liquid metals. (A) Size distribution of EGaIn nanoparticles (left) and their TEM image (left inset). SEM image of the particles after mechanical sintering (right). Reproduced with permission from ref[126]. Copyright 2015, WILEY-VCH Verlag GmbH & Co. KGaA, Weinheim; (B) SEM image of uncoalesced EGaIn nanoparticles (left inset) and coalesced EGaIn nanoparticles after laser sintering (left). Effect of laser fluence on the resistance of the EGaIn film with different particle diameters (right). Reproduced with permission from ref[128]. Copyright 2018, American Chemical Society; (C) Schematic illustration of the self-healing mechanism (left). Resistance change for the damage from a hole punch (right). Reproduced with permission from ref[131]. Copyright 2018, The Author(s); (D) Schematic illustration of the process used to create bGaIn (top): spray printing of EGaIn nanoparticles onto a silicon wafer (i); heating the deposited film (ii), (iii); cooling the film and transferring onto VHB or silicon substrates (iv). LED array with bGaIn electrical interconnects before and after stretching to 250% strain (bottom). Reproduced with permission from ref[133]. Copyright 2018, The Author(s), under exclusive license to Springer Nature Limited; (E) SEM image of the permeable LMFM after activation via pre-stretch (left). Resistance change of the LMFM as a function of the number of stretching cycles at different strains (right). Reproduced with permission from ref[137]. Copyright 2021, The Author(s), under exclusive license to Springer Nature Limited; (F) Cross-sectional schematic illustration of the water-assisted erasing process (left) and sheet resistance as a function of the number of writing/erasing cycles (right). Reproduced with permission from ref[138]. Copyright 2019, American Chemical Society. EGaIn: Eutectic gallium-indium; LMFM: liquid metal fiber mat; SEM: scanning electron microscopy.

By utilizing the coalescing behaviors of LM droplets, LM-based composites with electrically self-healing abilities have been reported[121,131,132]. In particular, Markvicka *et al.* developed an autonomously self-healing LM-PDMS composite with extraordinary electromechanical resilience[131]. The composite with high LM fractions (~50 vol%) was fabricated and electrically activated by mechanical sintering, exhibiting an electrical conductivity of ~1,000 S·cm^{-1}. When damage was induced to the composite, an alternative conductive pathway was created by autonomous and in situ coalescence of LM droplets around the damaged region [Figure 5C, left]. Hence, the composite was able to maintain its original electrical conductivity. The self-healing ability was demonstrated with cutting and puncturing experiments. The electrical resistance slightly increased or even decreased after subsequent damages were induced [Figure 5C, right]. This unexpected response was possible because of the electrical reconfiguration. In addition, the composite exhibited strain-insensitive properties so that an increase in electrical resistance was less than 10% at 50% strain. The electronically robust composite showed great potential in various applications, including soft robotics and wearable electronics.

Liu *et al.* thermally treated EGaIn nanoparticles and created a biphasic Ga-In (bGaIn), a printable conductor suitable for scalable manufacturing of highly stretchable electronic circuits[133]. bGaIn was made by spray-printing EGaIn nanoparticles [Figure 5D, i], heating them in a furnace for 30 min at 900 ℃, and cooling them. When heated, particles at the top surface transformed into crystalline solids due to oxidation and phase segregation [Figure 5D, ii], while underlying particles coalesced into conductive liquid paths [Figure 5D, iii]. The resulting bGaIn was transferred to a stretchable substrate, such as PDMS [Figure 5D, iv]. The solid oxide particles were evenly spread over the substrate, and the liquid EGaIn showed strong wettability to the solids, therefore exhibiting mechanical stability and excellent electromechanical performance. It showed an initial conductivity of 20,600 $S \cdot cm^{-1}$, and resistance increased only 6% at 100% strain on PDMS. In addition, bGaIn was employed to build robust connections with conventional rigid electronic components. When an electronic component was mounted on bGaIn, the liquid parts of bGaIn flowed to encompass the electronic component, while solid bGaIn particles secured the liquid bGaIn to the electronic component, resulting in the formation of a reliable electrical connection. As a consequence, stretchable circuit board assemblies, which operated even under large strains, could be fabricated by transfer-printing bGaIn traces and connecting electronic components, including resistors, capacitors, and light-emitting diodes [Figure 5D, bottom].

Although the LM itself is known to be highly biocompatible when used in wearable electronics, the non-breathable encapsulation is required to prevent leakage of the LM from the composite, which can cause skin irritations over long-term wearing[134-136]. Meanwhile, Ma *et al.* developed a highly permeable and superelastic conductor named "liquid metal fiber mat" (LMFM)[137]. The LMFM was fabricated by coating EGaIn on electrospun SBS, followed by repeating pre-stretching cycles to a strain of 1,800%. During the pre-stretching process, EGaIn was transferred into a mesh-like porous structure along the SBS microfibers and formed a vertically wrinkled structure [Figure 5E, left]. The lateral meshes and vertical wrinkles contributed to ultrahigh electrical stability and excellent permeability. For instance, the LMFM with an initial conductivity of ~100 $S \cdot cm^{-1}$ exhibited only a small increase in resistance when stretched to 1,800% [Figure 5E, right]. The air permeability (79.5 $mm \cdot s^{-1}$) and moisture permeability (724 $g \cdot m^{-2} \cdot day^{-1}$) of the LMFM were higher than those of commercial nylon cloth (11.8 $mm \cdot s^{-1}$ and 621 $g \cdot m^{-2} \cdot day^{-1}$) and a medical patch (7.0 $mm \cdot s^{-1}$ and 31 $g \cdot m^{-2} \cdot day^{-1}$). To evaluate the importance of permeability for long-term wearable applications, on-skin tests were conducted. In contrast to non-permeable materials, such as SBS, Ecoflex, and PDMS film, permeable LMFM did not cause any skin irritations (no erythema or edema).

LMs have also been combined with hydrogels to fabricate flexible, printable, and rewritable electronic circuits. For example, Park *et al.* demonstrated composites of EGaIn droplets and poly(ethylene glycol) diacrylate (PEGDA) hydrogel, in which EGaIn microparticles were vertically phase-segregated[138]. Friction on the composite surface with a high EGaIn population induced the removal of the covering PEGDA and rupturing of the oxide layers in the EGaIn microparticles, resulting in the formation of conductive pathways. When water was applied to the hydrogel, the surface was swollen, and the conductive pathway was removed [Figure 5F, left top]. After the water was dried, the surface was de-swollen and returned to its initial nonconductive state [Figure 5F, left bottom]. The writing/erasing/rewriting cyclic performance was examined, and the result showed that the hydrogel could endure over 20 rewritable cycles, with a tremendous change in electrical resistance from ~1 to ~10^7 Ω [Figure 5F, right]. Besides, the liquid-like properties of EGaIn imparted extra softness to the composite, making it suitable for a mechanically flexible 3D electrode.

LM-based nanocomposites have been extensively researched due to their outstanding stretchability and metal-like conductivity. By forming a percolation network through the coalescence of neighboring LM

droplets, they have been developed as self-healing, printable, permeable, or rewritable stretchable conductors. Despite their potential benefits, the field of LM-based composites remains relatively unexplored compared to carbon and metal-based nanocomposites. This is due to several challenges, including controlling the size of LM droplets, improving performance reliability, and preventing LM leakage. More research is needed to address these challenges and realize the full potential of LM-based nanocomposites for high-performance device applications.

BIO-INTEGRATED WEARABLE SENSORS BASED ON NANOCOMPOSITES

The conductive and stretchable nanocomposites mentioned above can be utilized in numerous applications, such as stretchable interconnects[139,140], wearable heaters[141], triboelectric nanogenerators (TENGs)[142], and skin-mounted sensors[143]. Most studies have focused on developing on-skin biosensing devices because the nanocomposites exhibit low Young's moduli, similar to that of human skin. These soft biosignal recording devices can adhere to the target parts of the human body with minimal mechanical mismatch and effectively record biosignals with high SNRs for long-term periods[144].

In this chapter, we review the application of nanocomposites in the fabrication of wearable biosignal recording sensors. The sensors are categorized into four different types: electrophysiological sensors, strain sensors, pressure sensors, and biochemical sensors. Electrophysiological sensors include EEG, ECG, and EMG sensors that require high SNRs for accurate signal analysis[145,146]. Strain and pressure sensors are applied to various parts of the body to read body motions or perceive external stimuli, of which their performance, such as high sensitivity, should be stable even under repetitive mechanical deformations[147-149]. Biochemical sensors, which typically utilize sweat to detect and quantify the concentrations of target biomolecules, such as glucose, also need to maintain high selectivity and sensitivity even under dynamically deformed situations[150]. Table 2 summarizes some research in recent years on the wearable sensors based on soft conductive nanocomposites, including their material components, sensing mechanisms, and sensing performances.

Electrophysiological sensors

Electrophysiological signals are essential for controlling our body and maintaining our health, as they represent the electrical activity of organs, such as the brain, heart, and muscles. To record these signals for healthcare, clinical, and research purposes, various wearable electronic devices, such as EEG, ECG, and EMG sensors, have been developed. Among them, soft conductive nanocomposites and their devices are particularly promising to overcome the limitations and challenges of the traditional rigid wearable electrophysiological sensors. Unlike rigid electrodes, devices made of soft nanocomposites can make conformal contact with skin tissue, avoiding air gaps[151] that could result in high electrical impedance and poor signal quality (i.e., SNR). The amplitude of electrophysiological signals collected through the skin is typically small, making them vulnerable to mechanical and electrical noise[55]. Therefore, conformal contact is crucial to reduce noise levels and improve the signal amplitude.

Researchers have explored different approaches to ensure conformal contact of devices with the skin. One effective method involves utilizing intrinsically soft organic materials instead of rigid metal materials to maximize softness[152]. Another key technique is to utilize the ultrathin thickness of the sensor, which lowers the stiffness and enables seamless integration with the curved skin[153]. Additionally, the application of conductive inks directly onto the skin enhances adhesion, avoiding air gaps[154].

Operational stability is another important factor to consider when fabricating electrophysiological sensors for long-term use[155]. Optimizing the mechanical properties so that the sensor can just withstand up to the

Table 2. Classification, mechanism, material, target, and performance of wearable sensors based on soft conductive nanocomposites

Sensor type	Material	Sensing mechanism	Mechanical properties	Target/Device location	Sensing performance	Ref.
Electrophysiological sensor	PEDOT:PSS, waterborne PU, D-sorbitol	-	Young's modulus ≈ 50 MPa, maximum strain = 43%, adhesion force = 0.43 $N \cdot cm^{-1}$	EEG (rear head), ECG (wrist and hand), EMG (wrist)	RMS noise < 38 μV under skin vibration, Identification of PQRST peaks in 20-40 dB	[152]
	AgNW, CNT, PDMS	-	Young's modulus ≈ 40 kPa, tolerant under 30% strain	EEG (ear canal)	Detection of alpha wave (8-13 Hz) and theta wave (3-7 Hz), separation of awake and drowsy states, detection of sleep onset	[158]
	Ag flake, PEDOT:PSS, Ion gels	-	Biaxial stretching (20%)	ECG (wrist), EMG (forearm)	Large SNR value (~50 dB), small SNR change (~1 dB) after sweating, durable over 7 h	[160]
	Ag microflake, EGaIn, SIS	-	Maximum strain ≈ 1,000%	ECG (chest)	Easy detection of R and T peaks, stable over 20 min	[161]
	AgNW, PEDOT:PSS	-	Young's modulus ≈ 8.8 MPa, maximum strain ≈ 60%	ECG (chest), EMG (forearm), bioimpedance (wrist)	Peak-to-peak voltage ≈ 2.56 mV (ECG), RMS noise ≈ 10.3 μV, SNR ≈ 10.9 dB (EMG)	[162]
	AgNW, SEBS	-	Maximum strain ≈ 540%	EMG (forearm)	Detection of clenching and bending, 16-channel recording	[44]
Strain sensor	AgNW, PDMS	Resistive	70% strain	Finger motion (glove)	GF = 2-14	[169]
	PANI, SEBS-g-MA	Resistive	Young's modulus ≈ 290 kPa, 300% strain	-	Sensing range = 0.5%-300%	[170]
	MWCNT, Ecoflex	Resistive	Stiffness = 166 kPa, 80% strain	Human-machine interface	Sensitivity = 1.61 from 0% to 40% strain, multi-point contact locations (error of 1.88 ± 0.95 mm in 30 mm × 30 mm area for a planar-shaped sensor)	[171]
	Carbon fiber, Epoxy resin, TPU	Resistive	> 30% strain	Hand motion (sleeve)	GF > 85,000 with a linearity (R^2) of 0.96, sensing range = 0%-3%	[172]
	MWCNT, AgNW, TPU	Resistive	Maximum strain ≈ 450%	Human motion	Sensing range = 0%-171%, GF ≈ 110,000 within 135%-171% strain	[167]
	CB, Graphene, CMC, paper	Resistive	Flexible	Human motion (finger, forearm)	GF ≈ 70, Sensing range = ± 1.0%	[173]
	CNT, PDMS	Resistive	> 100% strain	Human motion	GF ≈ 87 within 0%-40% strain, 6 within 40%-100% strain, detection of strain as low as 0.007%	[168]
Pressure sensor	GNP, PU	Piezoresistive	30% strain	Finger bending, voice vibration	Detection of pressure as low as 0.005 N (~50 Pa) and momentum as low as 1.9 mN·s	[70]
	PANI, PVDF	Piezoresistive	Flexible	Wrist pulse, respiration, throat vibration, gait motion	Sensitivity = 53 kPa^{-1}, sensing range = 58.4-960 Pa, response time = 38 ms	[180]
	PPy, AgNP, PDMS	Piezoresistive	Flexible	Finger pressure, respiration, acoustic vibrations	Sensitivity = 0.58 kPa^{-1} in 300-400 Pa	[183]
	CB-decorated fabric	Piezoresistive	Flexible	Blood pressure	Sensitivity = 0.1-0.5 kPa^{-1}, Sensing range = 0.5-25 kPa	[187]
	Gallium, PVA	Capacitive	Young's modulus = 217 MPa, maximum strain ≈ 540%, toughness =	Finger bending, Bicycle rolling	Sensitivity = 0.1 MPa^{-1} for < 0.6 MPa, 1.2 MPa^{-1} between 0.6 and 2.2 MPa, 0.2 MPa^{-1} for > 2.2 MPa	[188]

			74 MJ·m^{-3}			
	AgNW, CNT, PDMS, spandex fiber	Triboelectric	140% strain	Motion of heel	Sensitivity = 5.2 mV·Pa^{-1} for < 4 kPa, 0.39 mV·Pa^{-1} for > 4 kPa	[189]
Biochemical sensor	PANI, TEGO, PVA	Amperometric	Maximum strain ≈ 80%, toughness = 7.48 MJ·m^{-3}	Glucose (sweat)	0.2 uM to 10 mM glucose with a current gap of 2.1 μA	[196]
	Ni-Co MOF nanosheet, Ag, rGO/PU fiber	Amperometric	Maximum strain ≈ 100%	Glucose (sweat)	0.01 mM to 0.66 mM glucose with a sensitivity of 425.9 μA·mM·cm^{-2}	[197]
	EGaIn, PSS, CNT decorated with PtNP, SBS	Amperometric	-	Glucose, ethanol, lactate	0 to 0.5 mM glucose with a current gap of 1.9 μA, 0 to 2 mM ethanol, 0 to 5 mM lactate	[154]
	Au, CNT, AuNP, Ecoflex	Potentiometric	180° bending	Sodium ion (sweat)	Sensitivity = 55.5 mV decade^{-1}, Selectivity coefficient (K^+: -2.1, Ca^{2+}: -3.9)	[199]

AgNP: Silver nanoparticle; AgNW: silver nanowire; AuNP: gold nanoparticle; CB: carbon black; CMC: sodium carboxymethyl cellulose; CNT: carbon nanotube; ECG: electrocardiogram; EEG: electroencephalogram; EGaIn: eutectic gallium-indium; EMG: electromyogram; GF: gauge factor; GNP: graphene nanoplate; MOF: metal-organic framework; MWCNT: multi-walled carbon nanotube; PANI: polyaniline; PDMS: polydimethylsiloxane; PEDOT:PSS: poly(3,4-ethylenedioxythiophene):poly(styrene sulfonate); PPy: polypyrrole; PtNP: platinum nanoparticle; PU: polyurethane; PVA: poly(vinyl alcohol); PVDF: poly(vinylidene fluoride); RMS: root mean square; rGO: reduced graphene oxide; SBS: poly(styrene-butadiene-styrene); SEBS: poly(styrene-b-(ethylene-co-butylene)-b-styrene); SEBS-g-MA: poly-(styrene-co- ethylene-butylene-g-maleic-anhydride-co-styrene); SIS: styrene-isoprene block copolymer; SNR: signal-to-noise ratio; TEGO: thermally-exfoliated graphene oxide; TPU: thermoplastic polyurethane.

required strain is beneficial, as there is often a trade-off between electrical performance and stretchability. The application of soft and adhesive functionality can ensure stability, preventing detachment or failure of the device due to body motions[156,157]. Furthermore, achieving reproducibility under deformed conditions is necessary to facilitate accurate signal analysis. Considering the utilization of strain-insensitive materials in the sensor fabrication offers a promising solution to minimize unwanted noise and enhance sensing accuracy and operational stability.

Among various electrophysiological signals, the skin EEG signal provides information about overall brain activity, such as thinking, stress reception, and focus, rather than monitoring specific activities in small brain regions. Even so, conventional flat and rigid dry electrodes face challenges in acquiring high-quality EEG signals due to the presence of hair and the rough surface of the skin. Without conductive gels, imperfect contact causes significant degradation of signal quality. Alternative types of skin electrodes, such as 3D comb and canal electrodes, thereby, have been proposed. Soft nanocomposites have great potential when combined with these electrode design strategies. The nanocomposites can be easily fabricated into soft 3D structures and can make conformal contact with complicated structures, such as the ear canal.

Zhang *et al.* proposed a new type of dry electrode for long-term, motion-robust EEG monitoring by using organic materials that are highly biocompatible and suitable for use in sensitive skin areas[152]. The self-adhesive electrodes, which eliminate the need for additional adhesive materials, were fabricated by combining conductive (PEDOT:PSS) and nonconductive (waterborne PU and D-sorbitol) organic materials with a mold-casting fabrication process. The resulting electrodes have high electrical conductivity (approximately 400 S·cm^{-1} at 19 wt% PEDOT:PSS) and are highly conformable to the skin (~50 MPa at

19 wt% PEDOT:PSS), allowing for comfortable, long-term monitoring of biopotentials. For EEG recording, Zhang *et al.* designed the electrode with a 3D-comb structure and applied it to the occipital region of human subjects [Figure 6A][152]. The electrode successfully recorded the EEG signal pattern, which was highly activated in the occipital region during the open-eye period [Figure 6B]. The subject reported no notable complications during and after the measurement.

Meanwhile, Lee *et al.* reported a device for wireless real-time monitoring of electrophysiological signals by integrating a flexible conductive composite into a personal earphone [Figure 6C, left][158]. The researchers developed a flexible conductive composite comprising AgNWs, CNTs, and PDMS. The resulting material featured high electrical conductivity, excellent mechanical deformability, and biocompatibility, making it well-suited for use in wearable devices. The combination of AgNWs and CNTs contributed to lower impedance without sacrificing electrical conductivity, ensuring a high SNR for EEG recording. The EEG earphone was used to monitor the level of concentration of subjects and to wake them up when they entered a drowsy state of consciousness [Figure 6C, right].

In addition to monitoring brain activity, similar devices can be used to monitor the heart activity. The ECG signal provides valuable information about the electrical excitation tendencies of myocardial cells in the heart. Accurate diagnosis of cardiovascular diseases relies on identifying abnormal morphologies and temporal appearances of the characteristic peaks, including P, QRS, T, and U waves[159]. However, to precisely analyze these peaks amid motion noise, a soft electrode that can make conformal contact and provide high SNRs is required.

For example, electronic ink, which comprises Ag flakes, PEDOT:PSS, poly(3-hexylthiophene-2,5-diyl) (P3HT)-nanofibrils, and ion gels, can be drawn on the skin with a ballpoint pen to create such an electrode [Figure 6D][160]. The drawn electrode demonstrated a low sheet resistance of 1.2 $\Omega \cdot sq^{-1}$ under zero strain and 9.9 $\Omega \cdot sq^{-1}$ under 30% strain and mechanical reliability under repeated stretching (1,000 cycles of 10% strain). The electronic ink was printed on both wrists of a human subject to record ECG, and the shape of the electrode could deform along with the skin deformation (10%) with any visible damage [Figure 6E, left]. No significant differences were observed in the recorded ECG signals before and after the mechanical deformation [Figure 6E, right].

Recently, Zu *et al.* developed another electronic ink composed of Ag microflakes, EGaIn droplets, and a styrenic elastomer[161]. The Ag microflakes served not only as conductive fillers that increased the initial conductivity to as high as 6,380 $S \cdot cm^{-1}$ but also as bridging materials that prevented EGaIn droplets from being separated from each other under induced strain. This led to excellent electromechanical properties, with a relative resistance (R/R_0) of only 7.78 when stretched up to 1,000%. The electronic ink was printed on a TPU substrate as surface electrodes and directly contacted the human chest to acquire ECG signals. The researchers recorded ECG signals for over 20 min, detecting R and T peaks with ease [Figure 6F]. Conformal contact with the skin was maintained during recording, and the electrode caused no skin irritation. Additionally, the suitability of the electronic ink for stretchable digital circuits allowed it to be applied to interconnects for a wireless ECG monitoring system.

Lastly, there are examples of measuring muscle activities. EMG sensors are used to measure and record the electrical activity generated by skeletal muscles, providing valuable information on muscle function and the diagnosis of neuromuscular disorders. Unlike EEG and ECG, the subject has to activate the target muscles (i.e., move) to record EMG signals, which makes it challenging to record stable and high-quality EMG signals due to motion artifacts. For this reason, rigid needle electrodes that contact the muscle directly

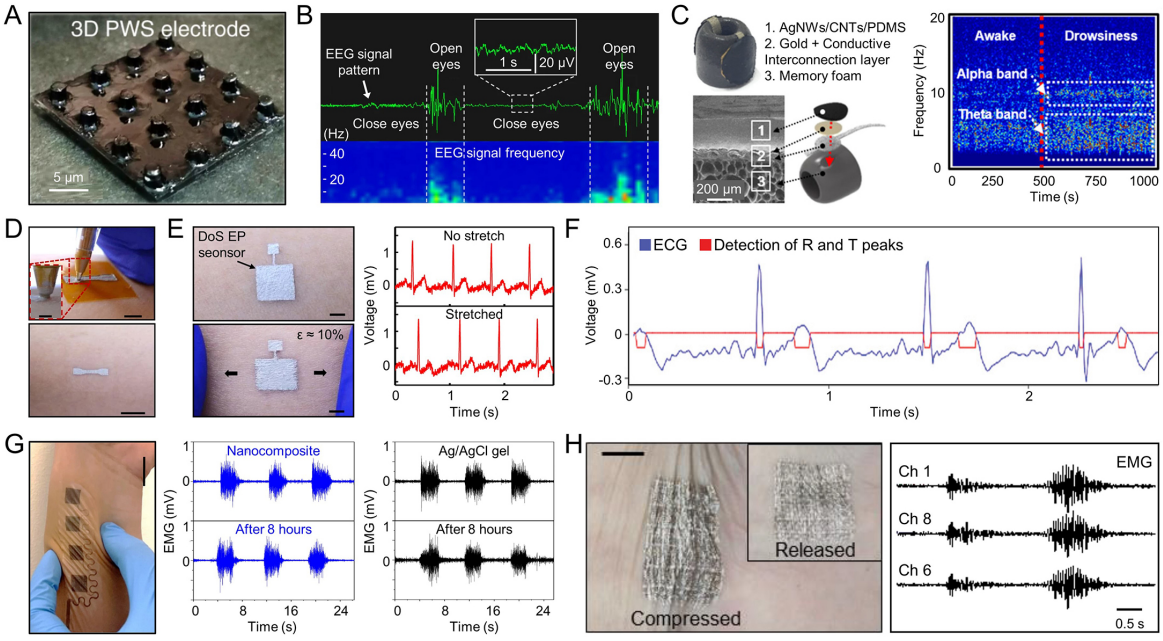

Figure 6. Electrophysiological sensors. (A) Image of a 3D-comb structured electrode; (B) EEG signals recorded during eye-blinking. Reproduced with permission from ref[152]. Copyright 2020, The Author(s); (C) Images of the structure and elements of the EEG earphone (left) and time-frequency analysis of EEG spectrogram from awake to drowsiness states (right). Reproduced with permission from ref[158]. Copyright 2018, American Chemical Society; (D) Stencil printing of the electronic ink (top) and the resulting electrode drawn directly on the skin (bottom); (E) Images of EP sensor (left) and recorded ECG signals (right) without and with applied strain. Reproduced with permission from ref[160]. Copyright 2020, The Author(s); (F) Analog voltage signals obtained from the Ag microflakes and EGaIn droplets-based ECG patch. Reproduced with permission from ref[161]. Copyright 2022, The Authors. Advanced Materials Technologies published by Wile-VCH GmbH; (G) Image of a nanocomposite electrode laminated on the forearm under applied strain (left). EMG signals measured with nanocomposite (middle) and Ag/AgCl gel electrode (right) before and after wearing for 8 h. Reproduced with permission from ref[162]. Copyright 2022, The Author(s); (H) Image of the skin-mounted sensor using patterned nanomembranes (left) and the recorded EMG data from three channels (right). Reproduced with permission from ref[44]. Copyright 2021, The American Association for the Advancement of Science. AgNWs: Silver nanowires; CNTs: carbon nanotubes; ECG: electrocardiogram; EEG: electroencephalogram; EGaIn: Eutectic gallium-indium; EMG: electromyogram; PDMS: polydimethylsiloxane.

through the skin have been widely used, as well as wet electrodes using conductive gels and adhesives. However, these needle electrodes can damage muscles and nerves and can induce electrode dislocation. To address these issues, recent research has focused on soft EMG sensors with high conductivity and conformal skin contact, for which soft conductive nanocomposites would be promising.

For instance, Namkoong *et al.* developed a conductive nanocomposite made of AgNWs and PEDOT:PSS, which is thin (~25 μm), moldable, and transferable to various substrates[162]. This nanocomposite was tested as a stretchable electrode and demonstrated high breathability and stable performance under external strain [Figure 6G, left]. The addition of AgNWs to PEDOT:PSS reduced the sheet resistance, and the addition of D-sorbitol lowered the Young's modulus. When compared to the conventional Ag/AgCl gel electrode, the AgNW/PEDOT:PSS electrode showed a similar initial SNR that increased over time (10.9 to 12.3 dB) [Figure 6G, middle], while the Ag/AgCl electrode showed a decreased SNR over time (10.6 to 7.5 dB) [Figure 6G, right].

More recently, Jung *et al.* presented a nanomembrane consisting of a single layer of aligned AgNWs that are half-embedded in an ultrathin SEBS membrane[44]. Spontaneous float-assembly of nanomaterials at the water-oil interface and the addition of a surfactant resulted in a highly packed AgNW layer. The

conductivity was further improved to 103,100 $S \cdot cm^{-1}$ (parallel to AgNW alignment) and 32,900 $S \cdot cm^{-1}$ (vertical to AgNW alignment) by cold welding. The nanomembrane maintained its conductivity up to 1,000% strain (in the vertical direction to AgNW alignment) and 400% strain (in the parallel direction to AgNW alignment). As the AgNWs were exposed to the surface of the nanomembrane, they could be patterned via conventional photolithography. Thanks to the high softness and ultrathin structure (~250 nm) of the nanomembrane, it could be applied to high-performance EMG sensors [Figure 6H].

Strain sensors

Strain sensing is important for wearable electronics as it enables the devices to detect and respond to changes in body position and movement. Wearable electronics, including fitness trackers and smartwatches, are designed to be worn on the body and provide information about physical activity and health. The addition of strain sensors allows these devices to accurately detect movement and exertion. Strain sensing is also crucial for the development of wearable robotics and prosthetics as it helps to control their movement and enables more natural and intuitive movement[163].

Strain sensors are divided into resistive, capacitive, and piezoelectric types according to their working mechanisms. In resistive strain sensors, the applied strain is measured by detecting the resistance variation during stretching deformations[164]. Capacitive strain sensors measure the capacitance change resulting from variation in the distance between two electrodes induced by strain. Piezoelectric strain sensors consist of piezoelectric materials that convert the mechanical deformation into the electrical potential.

Most of the strain sensors utilizing the soft conductive nanocomposites belong to the resistive type due to their simple structure, wide sensing range, and excellent reproducibility[165]. In resistive strain sensors, two main principles are involved: macroscopic deformation and nanoscopic deformation [Figure 7A]. Macroscopically, when a soft elastic material is stretched to a longer structure, it becomes thinner due to its Poisson's ratio, which increases its electrical resistivity. Nanoscopically, the limited conductive pathway and higher inter-nanomaterial resistivity increase the overall electrical resistivity when stretched. Additionally, the creation of microcrack structures through pre-stretching of the nanocomposites further enhances the operational range and sensitivity of sensors[166-168]. As the material deforms, the microcracks within it open or change their alignment, causing a significant microscopic alteration in the conductive pathways. This change magnifies the sensitivity of the strain sensor.

Low hysteresis is a crucial property for strain sensors, as well as high strain sensitivity. In 2014, Amjadi *et al.* demonstrated that a sandwich-structured nanocomposite consisting of AgNWs embedded between two PDMS layers was suitable for strain sensors due to its stretchability, sensitivity, and linearity[169]. This nanocomposite endured repeated strains of up to 40% with no hysteresis, preventing post-strain wrinkles that could deform the conductive pathway structure. Additionally, Amjadi *et al.* also demonstrated a wireless smart glove system using the nanocomposite strain sensor on the fingers [Figure 7B][169]. The computer-simulated finger avatar successfully mimicked the motion of real fingers with the smart glove.

Ensuring conformal integration between wearable strain sensors and the target region of the body is crucial for accurately representing body motion through strain sensing data. The moduli of the sensor and tissue should be matched to prevent erroneous readings. To address this challenge, conducting organic composites has been proposed, as demonstrated by Stoyanov *et al.*[170]. They developed an elastomer-like conductor based on PANI that is covalently bonded to maleic anhydride-grafted SEBS and then mixed it with SEBS. This block copolymer elastic conductor (BEC) exhibited excellent elastic and electrical properties, with a low Young's modulus reaching down to 290 kPa and high conductivity increasing up to

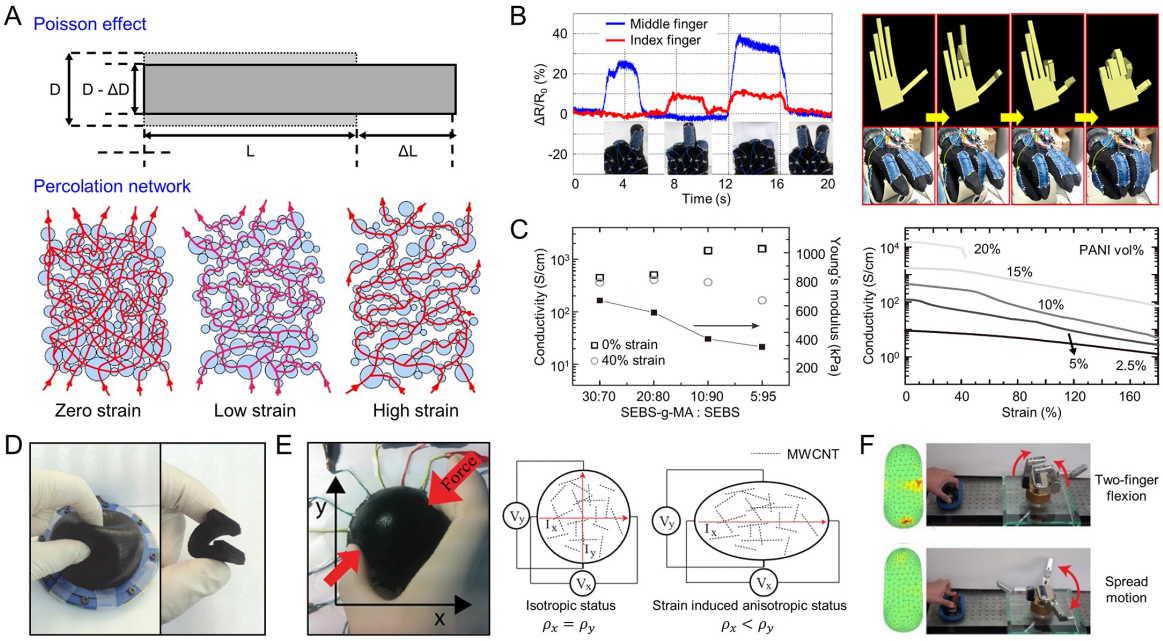

Figure 7. Strain sensors. (A) Schematic of the principle strain sensing mechanisms; (B) Motion detection of index and middle fingers (left) and control of avatar fingers using a wireless smart glove system (right). Reproduced with permission from ref[169]. Copyright 2014, American Chemical Society; (C) Conductivity and Young's modulus of the BEC at fixed PANI concentration [10% (v/v)] (left) and conductivity change under stretching for different amounts of PANI (right). Reproduced with permission from ref[170]. Copyright 2013, WILEY-VCH Verlag GmbH & Co. KGaA, Weinheim; (D) Deformation of the dome-shaped nanocomposite sensor under pinching and binding; (E) Multidirectional strain mapping test (left) and mechanism for distinguishing the direction of the strain (right); (F) Control of robotic finger motions using the strain sensor. Reproduced with permission from ref[171]. Copyright 2017, The Author(s). BEC: Block copolymer elastic conductor; MWCNT: multi-walled carbon nanotube; PANI: polyaniline; SEBS: poly[styrene-b-(ethylene-co-butylene)-b-styrene]; SEBS-g-MA: poly(styrene-co-ethylene-butylene-g-maleic-anhydride-co-styrene).

1.5×10^4 S·cm^{-1}, depending on the mixture ratio [Figure 7C, left]. Specifically, for 15% (v/v) PANI BEC, it retained a high level of conductivity over a wide strain range (100 S·cm^{-1} at 180% strain) [Figure 7C, right]. The BEC could be applied as capacitive strain sensors, which could precisely follow various strain profiles.

While the unidirectional strain sensors have been successful in recording the one-directional strain changes during the body motion, they may not be compatible with monitoring multidirectional motions, which is necessary for mapping the dynamic motion of the body. Lee *et al.* developed multidirectional strain mapping sensors based on a nanocomposite of MWCNTs and Ecoflex elastomer [Figure 7D][171]. By optimizing the sensor, 2.5 wt% MWCNTs with low stiffness (76 kPa) and high strain sensitivity (1.61, from 0% to 40% strain) were selected. Anisotropic electrical impedance tomography was used to analyze the internal resistivity distribution of the nanocomposite. Four electrical connections were selected and switched by the computer among the 16 electrode connections around the dome-shaped nanocomposite sensor. The deformation of the sensor caused resistivity changes between the electrode connections [Figure 7E]. A human-machine interface based on the MWCNT/Ecoflex strain sensor was demonstrated. The sensor recorded strain locations and intensities induced by five fingers, and the user could manipulate the robot hand with the multidirectional strain sensor for complicated motions, including one-finger folding, two-finger folding, and hand spreading [Figure 7F].

In another study conducted by Araromi *et al.*, ultra-sensitive strain sensors were developed by forming microstructures in an anisotropic conductive material consisting of orthogonally-stacked aligned-carbon-fiber/epoxy nanocomposite layers[172]. The researchers carved the anisotropic conductive material into a periodic structure that is deformable under external stress. The microstructure exhibits high initial resistance under no stress, but under compression, the conduction pathways are shortened, resulting in low resistance. Conversely, under extension, the conduction pathways are saturated, resulting in higher resistance. The sensor exhibited ultra-high sensitivity, with a gauge factor greater than 9,000 at high linearity ($R^2 > 0.98$) and greater than 85,000 at lower linearity ($R^2 > 0.96$). This material was used to develop a textile-based sensor-integrated sleeve to detect hand motion. The customized sleeve strain sensor successfully detected various hand and wrist motions.

Sun *et al.* developed an ultrasensitive strain sensor utilizing a microcrack structure[167]. MWCNTs and AgNWs were deposited on the electrospun TPU nanofiber, and the composite was slowly pre-stretched to 100% strain to create the microcrack structure. The microcracks divided the conductive layer into separate islands, forming an island-bridge structure. When the sensor was stretched, the bridges became longer, and the area of the islands increased, resulting in an increase in the resistance. Notably, as conductive pathways dramatically decreased due to crack propagation at high strains, resistance increased exponentially with the applied strain. Based on these mechanisms, the sensor achieved both high sensitivity and a wide operational range, exhibiting a gauge factor greater than 110,000 within the strain range of 135% to 171%. The sensor successfully captured weak signals, such as airflow impacts, and strong signals, such as large-scale human motions.

Paper-based sensors have gained significant attention as next-generation flexible sensors due to their various advantages, including disposable, inexpensive, lightweight, and easily available nature[173-177]. For example, Yun *et al.* developed a paper-based strain sensor composed of a paper substrate and a CB/graphene/sodium carboxymethyl cellulose (CMC) conductive layer[173]. By utilizing ionic CMC as a bridge to enhance the interaction between CB and graphene, electrical conductivity and corresponding sensitivity of the sensor were improved. It exhibited high sensitivity with a gauge factor exceeding 70 and could demonstrate mechanical durability (> 10,000 cycles). In addition, the sensor overcame its vulnerability to water by coating it with hydrophobic silica nanoparticles, enabling it to maintain its sensing performance even under wet conditions.

Pressure sensors

Pressure sensors fabricated with soft nanocomposites are another key component of the bio-integrated smart electronics[178,179]. Pressure sensors enable the detection of a wide range of body motions, from subtle finger touches to large limb motions, through one of the following mechanisms: piezoresistive, piezoelectric, capacitive, and triboelectric. Similar to the case of strain sensors, various types of nanofillers have been applied to develop highly sensitive soft pressure sensors[104].

Since the nanofillers introduced in this review are all conductive, pressure sensors made with these conductive nanofillers mostly correspond to the piezoresistive type. Piezoresistive pressure sensors rely on the resistance change caused by the deformation of their shape under applied pressure. If a dielectric layer is introduced between two conductive nanocomposites, capacitive-type pressure sensors can be fabricated. In this case, the capacitance changes as the two electrodes come closer under applied pressure. Also, if different material layers, capable of generating charges through rubbing or contacts, are incorporated with the conductive nanocomposites, triboelectric-type pressure sensors can be fabricated[156]. Piezoelectric-type pressure sensors require piezoelectric materials, either inorganic or organic, of which an electric dipole is

formed under external forces and charges are transported through the external circuit.

In the example provided by Wu *et al.*, a piezoresistive type pressure sensor was developed by using a GNP/ PU nanocomposite film covered with PDMS layers[70]. When a mechanical force was applied to the surface of the GNP/PU film, the film was elongated, which increased the total length of the current path and resulted in higher resistance [Figure 8A, left]. The sensor demonstrated high sensitivity, which could detect forces as low as 5 mN, and was able to sense various movements with a quick response time of less than 0.5 s. The sensor was also successful in detecting random hits by fingers [Figure 8A, right].

Piezoresistive-type pressure sensors have also been fabricated by using conductive polymers, such as PANI[180,181] and PPy[182]. For example, Yang *et al.* developed a flexible pressure sensor based on PANI for wearable applications[180]. Firstly, PANI was oxidatively polymerized in situ on electrospun polyvinylidene fluoride (PVDF) nanofibers. The resulting hierarchical PANI/PVDF nanofiber (HPPNF) film was then sandwiched between two electrode planes to function as a piezoresistive device [Figure 8B, left]. Although made of polymers, the pressure sensor showed a high sensitivity of 53 kPa^{-1} within the range of 58.4 to 960 Pa and exhibited a rather fast response time of 38 ms and high cycle stability (> 50,000 cycles). It could efficiently detect gait motion signals and identify different phases of walking, running, and jumping [Figure 8B, right].

Wang *et al.* developed a PPy/AgNP-based piezoresistive pressure sensor for monitoring respiration states on a mask[183]. First, they fabricated a PPy/AgNP hybrid film by irradiating an aqueous solution of pyrrole and silver nitrate with ultraviolet (UV) light [Figure 8C, left]. After 3 h of UV irradiation, short chains of PPy and AgNPs were formed. Then, additional PPy short chains, residual pyrrole, and Ag ions aggregated at the surface of AgNPs to form the final PPy/AgNP hybrid film at the air/water interface. The thickness of the film was 220 nm, and the AgNPs had an average diameter of 50 nm. To apply this hybrid film as a pressure sensor, it was placed between two micropatterned PDMS films. The sensor demonstrated stable resistance change during 1,000 bending cycles and could be stretched repeatedly to 20% strain. Its sensitivity ranged from 0.4 to 0.58 kPa^{-1} for pressures of 100-400 Pa. When attached to a mask, it detected changes in breathing patterns, whether shallow or deep [Figure 8C, right].

Continuous monitoring of BP in daily life is beneficial for understanding the relationship between the lifestyle and a variety of diseases of an individual, such as cardiovascular[184], cerebrovascular[185], and respiratory diseases[186]. However, conventional BP sensors are bulky, incompatible with the elastic and curved skin, and often inaccurate, which interrupts continuous and long-term monitoring of BP. Therefore, Luo *et al.* developed a skin-attachable, continuous BP monitoring system by combining a flexible piezoresistive sensor (FPS) and ECG sensors[187]. Inside the FPS, the number of contact points between CB nanoparticle-decorated fabric and the underlying gold electrode changed depending on the applied pressure, which imparted piezoresistive characteristics to the flexible device [Figure 8D, left]. The system calculated BP using the time difference between the wrist pulse signals from the FPS and the ECG signals. As a result, the researchers obtained BP values that coincided with those measured from a conventional device [Figure 8D, right]. Notably, the FPS-based device only consumed 3 nW to operate, allowing continuous and real-time BP monitoring with minimum power consumption.

Lou *et al.* prepared a highly resilient capacitive pressure sensor by layering LM-PVA films[188]. The LM-PVA film was fabricated by uniformly dispersing LM droplets in a PVA matrix, which were bound through hydrogen bonding between the hydroxyl group of PVA and the oxide layer of the LM droplets. The LM droplets improved the mechanical properties of the film, resulting in a 12.3-fold increase in toughness

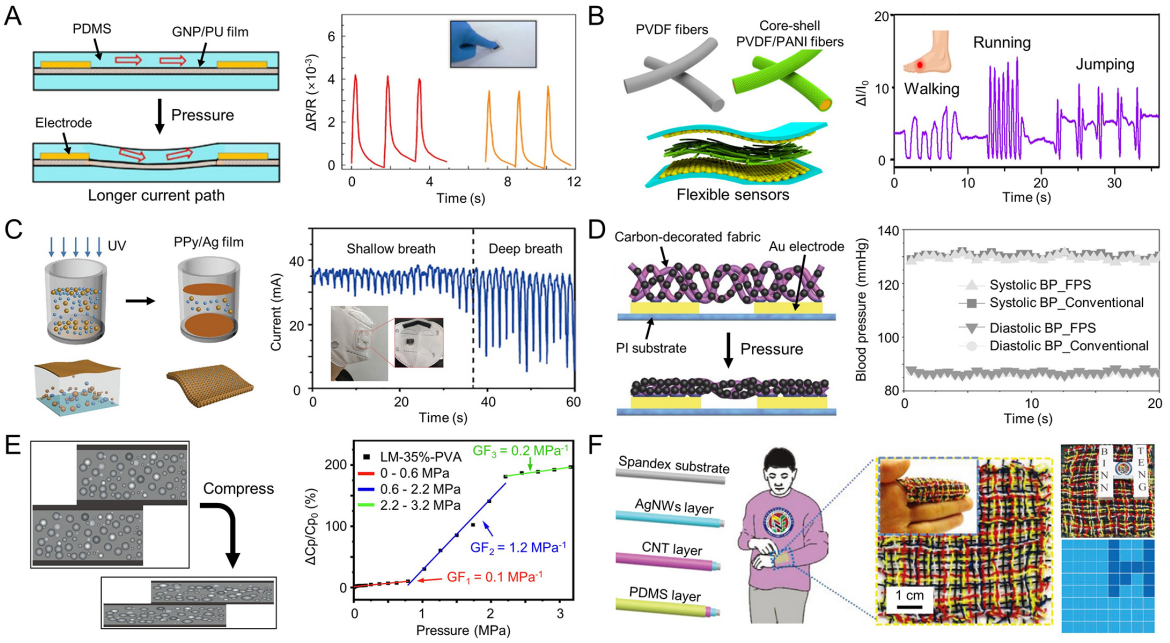

Figure 8. Pressure sensors. (A) Schematic illustration of resistive sensing mechanism (left) and relative resistance change of the GNP/PU film with finger pressures (right). Reproduced with permission from ref[70]. Copyright 2017, American Chemical Society; (B) Schematic illustration of the flexible pressure sensor based on PVDF/PANI nanofibers (left) and relative current response for different gaits (right). Reproduced with permission from ref[180]. Copyright 2021, American Chemical Society; (C) Schematic illustration of the PPy/AgNP hybrid film through interfacial photopolymerization (left) and detection of respiration rate with different breathing patterns using the film as a pressure sensor (right). Reproduced with permission from ref[183]. Copyright 2021, Elsevier B.V; (D) Materials and device structure of the FPS with and without applied pressure (left). Blood pressure obtained from the FPS and conventional photoplethysmogram sensor (right). Reproduced with permission from ref[187]. Copyright 2015, WILEY-VCH Verlag GmbH & Co. KGaA, Weinheim; (E) Schematic illustration of stacked LM-PVA films under pressing (left) and relative capacitance change with increasing pressure (right). Reproduced with permission from ref[188]. Copyright 2020, Elsevier B.V; (F) Preparation of the F-TENGs and structural representation of the F-TENG-based tactile sensor arrays (middle). Image of the sensor array with an H-shaped object and corresponding pressure distributions (right). Reproduced with permission from ref[189]. Copyright 2020, Wiley-VCH GmbH. AgNP: Silver nanoparticle; AgNWs: silver nanowires; BP: blood pressure; CNT: carbon nanotube; FPS: flexible piezoresistive sensor; F-TENG: fiber-shaped triboelectric nanogenerator; GF: gauge factor; GNP: graphite nanoplate; PANI: polyaniline; PDMS: polydimethylsiloxane; PPy: polypyrrole; PU: polyurethane; PVA: poly(vinyl alcohol); PVDF: polyvinylidene fluoride; UV: ultraviolet.

(74 MJ·m^{-3}). Two LM-PVA films were stacked, forming a parallel-plate capacitor. When external force was applied, the LM droplets were compressed, increasing the conductive area, reducing the gap between films, and increasing capacitance [Figure 8E, left]. The sensor demonstrated three levels of sensitivity (MPa^{-1}) based on the range of applied pressures [Figure 8E, right].

Ning *et al.* developed a pressure sensor array using fiber-shaped TENGs (F-TENGs)[189]. Firstly, they fabricated a single fiber with a diameter of 0.63 mm by consecutively depositing AgNWs, CNTs, and PDMS on a stretchable spandex fiber [Figure 8F, left]. The fiber exhibited high stretchability of up to 140% and could be knotted, folded, and woven into textiles. It showed negligible performance change even after agitation in a beaker with detergent and water. When used as a pressure sensor, a taping force of 1 N generated the maximum open circuit voltage of 10 V. The sensitivity of the sensor was 5.2 and 0.39 mV·Pa^{-1} for tapping forces less than and greater than 4 kPa, respectively. For the wearable device applications, F-TENGs were woven into an 8 × 8 sensor array [Figure 8F, middle]. Each of the eight F-TENGs was placed as weft and warp yarns with a spacing of three common fibers. Then, the 16 voltage signals were recorded using the multichannel data acquisition system. This sensor array could detect the pressure distribution

applied by an H-shaped object in real time [Figure 8F, right].

Biochemical sensors

Point-of-care biochemical detection is vital for a complete assessment of the health status of an individual. The ability to monitor metabolites and electrolytes in sweat, tears, and saliva provides valuable information for diagnosing and monitoring various diseases. For instance, glucose monitoring is essential for diabetic patients[190], while lactate monitoring is vital for athletes and critically ill patients[191]. Electrolyte monitoring, such as sodium and potassium, is also essential for patients with kidney and cardiovascular diseases[192]. To detect these biomarkers, antigen-antibody or enzymatic reactions are commonly used[193], which induce electrical signal changes. Skin-interfaced biochemical sensors that use nanocomposites have been developed to improve the selectivity and sensitivity of these sensors[194,195]. These sensors have a high potential for clinical applications due to their non-invasive and convenient nature.

Garg *et al.* successfully detected the glucose concentration in sweat using a PANI-based double polymer network nanocomposite[196]. The nanocomposite comprised PVA as the primary matrix, conductive PANI, and thermally-exfoliated GO (TEGO) as a conductive reinforcement. PANI not only served as a conductive material but also enhanced thermal and electrochemical stabilities. The nanocomposite had a hierarchical design where the nano-metric scale structure contributed to electrical conductance while the microscopic level contributed considerably to the mechanical and electrochemical properties [Figure 9A, left]. The nanocomposite exhibited superior mechanical strength of up to 7.7 MPa and toughness of 7.48 $MJ \cdot m^{-3}$ but had a rather low electrical conductivity of 0.14 $S \cdot m^{-1}$. Glucose oxidase was stably immobilized on the nanocomposite due to its high porosity and large surface area, making it a prototype for a non-invasive glucose sensor. Cyclic voltammetry revealed its pseudo-capacitive behavior with a redox peak potential between -0.4 and -0.6 V. In a test with a glucose concentration ranging from 0.2 μM to 10 mM, the sensor could detect glucose concentrations as low as 0.2 μM with a wide current gap of 2.1 μA [Figure 9A, right].

In another example, Shu *et al.* developed a glucose sensor using Ni-Co metal-organic framework (Ni-Co MOF) nanosheets[197]. The researchers coated the Ni-Co MOF nanosheets on a highly stretchable rGO/PU fiber using Ag conductive glue [Figure 9B, left]. The fiber had a diameter of approximately 1 mm, and the length of Ni-Co MOF nanosheets was hundreds of nanometers. This fiber electrode exhibited stable electrochemical properties, with its oxidation peak reducing by only 19.9% under 100% strain and the redox peak current remaining consistent even after 10,000 cycles of 20% strain. Specifically, this sensor could detect glucose concentrations ranging from 10 μM to 0.66 mM with a high sensitivity of 425.9 $\mu A \cdot mM^{-1} \cdot cm^{-2}$. By creating a three-electrode system with this fiber and absorbent fabric, it could function as a real-time glucose monitor attached to human skin [Figure 9B, middle]. The sensor detected changes in glucose levels in sweat throughout the day, which closely matched the data obtained from a commercial glucose meter [Figure 9B, right].

In another example, the concentrations of various metabolites in sweat could be quantified using LM particles coated with PSS and Pt-decorated CNTs (CMPs). Lee *et al.* developed CMP-based electrodes that not only enhanced mechanical stability, conductivity, and processability over bare LM particle-based electrodes but also enabled enzyme immobilization by the carboxyl group of CNTs[154]. Biochemical sensors were prepared by immobilizing the relevant redox enzyme (e.g., glucose oxidase, alcohol oxidase, and lactate oxidase) on stencil-printed CMP-based electrodes [Figure 9C, left]. The sensors measured current changes induced by enzymatic reactions and showed a linear response to the amount of change of target metabolites with a high linearity of $R^2 > 0.98$ [Figure 9C, right]. The chemical stability and selectivity of the sensors were examined, supporting the reliability of wearable biochemical sensors.

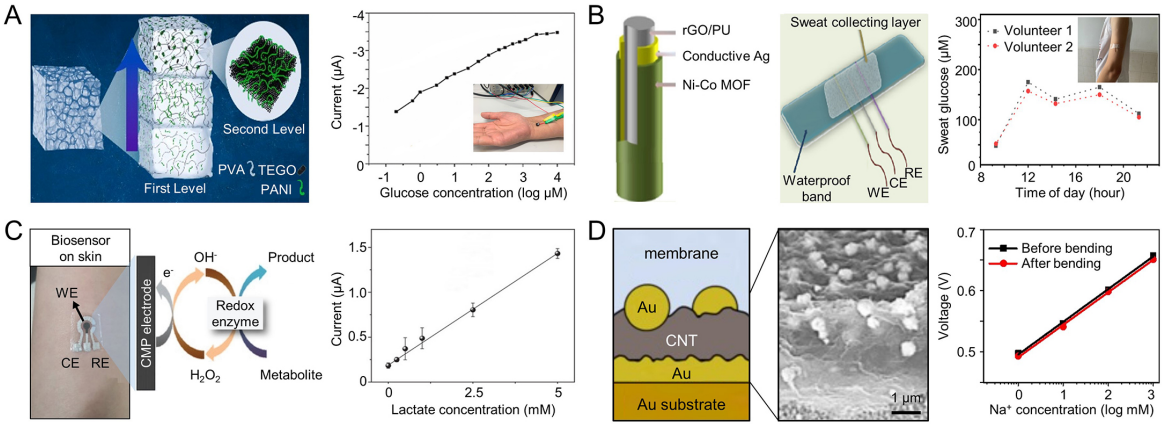

Figure 9. Biochemical sensors. (A) Schematic of the PANI-based hierarchically designed nanocomposite (left) and current level according to the concentration of glucose (right). Reproduced with permission from ref[196]. Copyright 2021, Elsevier Ltd; (B) Schematic of the Ni-Co MOF nanosheet coated rGO/PU fiber (left) and the glucose sensor integrated into the elastic fabric (middle). Measured glucose content in sweat by the wearable sensor for one day (right). Reproduced with permission from ref[197]. Copyright 2021, American Chemical Society; (C) Image and mechanism of the CMP-based biochemical sensor (left). Current level according to the concentration of lactate (right). Reproduced with permission from ref[154]. Copyright 2022, Wiley-VCH GmbH; (D) Schematic illustration and SEM image of the Au/SWCNT/AuNPs composite (left). Voltage level according to the concentration of sodium before and after 500 bending cycles (right). Reproduced with permission from ref[199]. Copyright 2021, Elsevier B.V. AuNPs: Gold nanoparticles; CE: counter electrode; CMP: Pt-decorated CNT; CNT: carbon nanotube; MOF: metal-organic framework; PANI: polyaniline; PU: polyurethane; PVA: poly(vinyl alcohol); RE: reference electrode; rGO: reduced graphene oxide; SWCNT: multi-walled carbon nanotube; TEGO: thermally-exfoliated GO; WE: working electrode.

Sodium ions are relevant to the hydration status and can be utilized as a biomarker for diagnosing stroke and kidney issues[198]. Lim *et al.* fabricated a sodium sensor using Au/SWCNT/AuNPs nanocomposites as ion-selective electrodes[199]. The Au pad at the bottom aided in material integration without delamination, while the AuNPs at the top contributed to a higher capacitance and larger surface area, resulting in highly sensitive and stable sodium concentration measurements [Figure 9D, left]. By integrating the Au/SWCNT/AuNPs electrode with a thin-film circuit, a wireless, flexible, and real-time on-skin sodium sensor could be developed [Figure 9D, right]. The entire sensor demonstrated a sensitivity of 55.5 mV decade^{-1} and high mechanical stability, with stable performance after 500 bending cycles.

CONCLUSION AND OUTLOOK

Numerous studies over the past decade have focused on developing soft conductive nanocomposites for wearable biosignal recording devices. These materials have much lower Young's moduli than conventional rigid electronic materials, making them ideal for wearable sensors that conform to the shape of the human body. By reducing mechanical mismatch, soft nanocomposites help mitigate side effects that frequently occur with rigid wearable electronics when attached to the soft curvilinear human body.

Material characteristics of nanocomposites vary significantly depending on the types of nanofiller incorporated, such as carbon-based nanomaterials, CPs, metal-based nanomaterials, and LMs[200-202]. Each filler has been successfully incorporated into a soft matrix and further optimized for use as soft wearable sensors, including electrophysiological, strain, pressure, and biochemical sensors. However, it is still challenging to achieve both high conductivity and softness simultaneously because excessive nanofiller loading leads to degradation of the soft mechanical property. Moreover, the intrinsic viscoelasticity of polymeric matrices causes electrical and mechanical hysteresis, making them susceptible to long-term repeated use.

To address the aforementioned challenges and enhance the performance of the on-skin biosignal recording, it is crucial to prioritize the advancement of long-term stability and mechanical robustness while retaining high conductivity. As previously discussed, LMs offer a promising approach to fabricating composites with minimal hysteresis, as they have a minimal impact on the mechanical properties of polymeric matrices. Also, paper-based electronics integrated with nanomaterials can be a promising candidate in wearable electronic fields due to their lightweight, environmental friendliness, and biodegradability. Moreover, the integration of machine learning and numerical simulation technology can provide a viable means of exploring suitable materials and fabrication methodologies for nanocomposites used in wearable devices. By implementing such technologies to improve material and device performance, soft nanocomposites with high sensitivity and durability will be further employed in bio-integrated electronics.

DECLARATIONS

Acknowledgments

This work was supported by the Institute for Basic Science (IBS-R006-A1). This research was supported by the KERI Primary research program of MSIT/NST (No. 23A01064)

Authors' contributions

Nam S, Park C, and Sunwoo SH contributed equally.
Outlined the manuscript structure: Nam S, Park C, Kim M, Lee H
Conducted the literature review and wrote the manuscript: Nam S, Park C, Sunwoo SH
Reviewed and revised the manuscript: Kim DH, Lee M

Availability of data and materials

Not applicable.

Financial support and sponsorship

This work was supported by the Institute for Basic Science (IBS-R006-A1). This research was supported by the KERI Primary research program of MSIT/NST (No. 23A01064).

Conflicts of interest

All authors declared that there are no conflicts of interest.

Ethical approval and consent to participate

Not applicable.

Consent for publication

Not applicable.

REFERENCES

1. Cho KW, Lee WH, Kim BS, Kim DH. Sensors in heart-on-a-chip: a review on recent progress. *Talanta* 2020;219:121269. DOI PubMed
2. Sunwoo S, Han SI, Joo H, et al. Advances in soft bioelectronics for brain research and clinical neuroengineering. *Matter* 2020;3:1923-47. DOI
3. Squair JW, Gautier M, Mahe L, et al. Neuroprosthetic baroreflex controls haemodynamics after spinal cord injury. *Nature* 2021;590:308-14. DOI PubMed
4. Hong YJ, Lee H, Kim J, et al. Multifunctional wearable system that integrates sweat-based sensing and vital-sign monitoring to

estimate pre-/post-exercise glucose levels. *Adv Funct Mater* 2018;28:1805754. DOI

5. Song J, Son D, Kim J, et al. Wearable force touch sensor array using a flexible and transparent electrode. *Adv Funct Mater* 2017;27:1605286. DOI
6. Hua Q, Sun J, Liu H, et al. Skin-inspired highly stretchable and conformable matrix networks for multifunctional sensing. *Nat Commun* 2018;9:244. DOI PubMed PMC
7. Konstantinidis D, Iliakis P, Tatakis F, et al. Wearable blood pressure measurement devices and new approaches in hypertension management: the digital era. *J Hum Hypertens* 2022;36:945-51. DOI PubMed PMC
8. Choi MK, Park OK, Choi C, et al. Cephalopod-inspired miniaturized suction cups for smart medical skin. *Adv Healthc Mater* 2016;5:80-7. DOI
9. Sunwoo SH, Cha MJ, Han SI, et al. Ventricular tachyarrhythmia treatment and prevention by subthreshold stimulation with stretchable epicardial multichannel electrode array. *Sci Adv* 2023;9:eadf6856. DOI PubMed PMC
10. Kim HJ, Jung D, Sunwoo S, Jung S, Koo JH, Kim D. Integration of conductive nanocomposites and nanomembranes for high□performance stretchable conductors. *Adv Nanobiomed Res* 2023;3:2200153. DOI
11. Hong YJ, Jeong H, Cho KW, Lu N, Kim D. Wearable and implantable devices for cardiovascular healthcare: from monitoring to therapy based on flexible and stretchable electronics. *Adv Funct Mater* 2019;29:1808247. DOI
12. Kim SJ, Cho KW, Cho HR, et al. Stretchable and transparent biointerface using cell-sheet-graphene hybrid for electrophysiology and therapy of skeletal muscle. *Adv Funct Mater* 2016;26:3207-17. DOI
13. Joo H, Lee Y, Kim J, et al. Soft implantable drug delivery device integrated wirelessly with wearable devices to treat fatal seizures. *Sci Adv* 2021;7:eabd4639. DOI PubMed PMC
14. Lee H, Choi TK, Lee YB, et al. A graphene-based electrochemical device with thermoresponsive microneedles for diabetes monitoring and therapy. *Nat Nanotechnol* 2016;11:566-72. DOI
15. Lee H, Song C, Hong YS, et al. Wearable/disposable sweat-based glucose monitoring device with multistage transdermal drug delivery module. *Sci Adv* 2017;3:e1601314. DOI PubMed PMC
16. Park C, Kim MS, Kim HH, et al. Stretchable conductive nanocomposites and their applications in wearable devices. *Appl Phys Rev* 2022;9:021312. DOI
17. Kim H, Yoo S, Joo H, et al. Wide-range robust wireless power transfer using heterogeneously coupled and flippable neutrals in parity-time symmetry. *Sci Adv* 2022;8:eabo4610. DOI PubMed PMC
18. Lee M, Shim HJ, Choi C, Kim DH. Soft high-resolution neural interfacing probes: materials and design approaches. *Nano Lett* 2019;19:2741-9. DOI PubMed
19. Yoo S, Lee J, Joo H, Sunwoo SH, Kim S, Kim DH. Wireless power transfer and telemetry for implantable bioelectronics. *Adv Healthc Mater* 2021;10:e2100614. DOI
20. Sunwoo SH, Ha KH, Lee S, Lu N, Kim DH. Wearable and implantable soft bioelectronics: device designs and material strategies. *Annu Rev Chem Biomol Eng* 2021;12:359-91. DOI PubMed
21. Zhang H, Xie L, Shen X, et al. Catechol/polyethyleneimine conversion coating with enhanced corrosion protection of magnesium alloys: potential applications for vascular implants. *J Mater Chem B* 2018;6:6936-49. DOI
22. Morais LS, Serra GG, Muller CA, et al. Titanium alloy mini-implants for orthodontic anchorage: immediate loading and metal ion release. *Acta Biomater* 2007;3:331-9. DOI
23. Kaltenbrunner M, Sekitani T, Reeder J, et al. An ultra-lightweight design for imperceptible plastic electronics. *Nature* 2013;499:458-63. DOI
24. Shim HJ, Sunwoo SH, Kim Y, Koo JH, Kim DH. Functionalized elastomers for intrinsically soft and biointegrated electronics. *Adv Healthc Mater* 2021;10:e2002105. DOI
25. Zhou Y, Wan C, Yang Y, et al. Highly stretchable, elastic, and ionic conductive hydrogel for artificial soft electronics. *Adv Funct Mater* 2019;29:1806220. DOI
26. Kang T, Cha GD, Park OK, et al. Penetrative and sustained drug delivery using injectable hydrogel nanocomposites for postsurgical brain tumor treatment. *ACS Nano* 2023;17:5435-47. DOI
27. Lim C, Hong YJ, Jung J, et al. Tissue-like skin-device interface for wearable bioelectronics by using ultrasoft, mass-permeable, and low-impedance hydrogels. *Sci Adv* 2021;7:eabd3716. DOI PubMed PMC
28. Cha GD, Lee WH, Sunwoo SH, et al. Multifunctional injectable hydrogel for *in vivo* diagnostic and therapeutic applications. *ACS Nano* 2022;16:554-67. DOI PubMed
29. Lim C, Shin Y, Jung J, Kim JH, Lee S, Kim D. Stretchable conductive nanocomposite based on alginate hydrogel and silver nanowires for wearable electronics. *APL Mater* 2019;7:031502. DOI
30. Yuk H, Lu B, Zhao X. Hydrogel bioelectronics. *Chem Soc Rev* 2019;48:1642-67. DOI PubMed
31. Koo JH, Kang J, Lee S, et al. A vacuum-deposited polymer dielectric for wafer-scale stretchable electronics. *Nat Electron* 2023;6:137-45. DOI
32. Song JK, Kim J, Yoon J, et al. Stretchable colour-sensitive quantum dot nanocomposites for shape-tunable multiplexed phototransistor arrays. *Nat Nanotechnol* 2022;17:849-56. DOI
33. Cho KW, Sunwoo SH, Hong YJ, et al. Soft bioelectronics based on nanomaterials. *Chem Rev* 2022;122:5068-143. DOI
34. Jung D, Lim C, Park C, et al. Adaptive self-organization of nanomaterials enables strain-insensitive resistance of stretchable metallic nanocomposites. *Adv Mater* 2022;34:e2200980. DOI PubMed

35. Park J, Choi S, Janardhan AH, et al. Electromechanical cardioplasty using a wrapped elasto-conductive epicardial mesh. *Sci Transl Med* 2016;8:344ra86. DOI
36. Lee W, Yun H, Song J, Sunwoo S, Kim D. Nanoscale materials and deformable device designs for bioinspired and biointegrated electronics. *Acc Mater Res* 2021;2:266-81. DOI
37. Sunwoo SH, Han SI, Jung D, et al. Stretchable low-impedance conductor with Ag-Au-Pt core-shell-shell nanowires and in situ formed Pt nanoparticles for wearable and implantable device. *ACS Nano* 2023;17:7550-61. DOI PubMed
38. Sunwoo S, Han SI, Kang H, et al. Stretchable low-impedance nanocomposite comprised of Ag-Au core-shell nanowires and Pt black for epicardial recording and stimulation. *Adv Mater Technol* 2020;5:1900768. DOI
39. Cha GD, Lee WH, Lim C, Choi MK, Kim DH. Materials engineering, processing, and device application of hydrogel nanocomposites. *Nanoscale* 2020;12:10456-73. DOI PubMed
40. Choi S, Han SI, Kim D, Hyeon T, Kim DH. High-performance stretchable conductive nanocomposites: materials, processes, and device applications. *Chem Soc Rev* 2019;48:1566-95. DOI
41. Joo H, Jung D, Sunwoo SH, Koo JH, Kim DH. Material design and fabrication strategies for stretchable metallic nanocomposites. *Small* 2020;16:1906270. DOI
42. Kim DC, Shim HJ, Lee W, Koo JH, Kim DH. Material-based approaches for the fabrication of stretchable electronics. *Adv Mater* 2020;32:e1902743. DOI PubMed
43. Hong S, Lee J, Do K, et al. Stretchable electrode based on laterally combed carbon nanotubes for wearable energy harvesting and storage devices. *Adv Funct Mater* 2017;27:1704353. DOI
44. Jung D, Lim C, Shim HJ, et al. Highly conductive and elastic nanomembrane for skin electronics. *Science* 2021;373:1022-6. DOI
45. Niu X, Peng S, Liu L, Wen W, Sheng P. Characterizing and patterning of PDMS-based conducting composites. *Adv Mater* 2007;19:2682-6. DOI
46. Lv R, Xu W, Na B, Chen B. Insight into the role of filler network in the viscoelasticity of a carbon black filled thermoplastic elastomer: a strain dependent electrical conductivity study. *J Macromol Sci* 2008;47:774-82. DOI
47. Kong J, Jang N, Kim S, Kim J. Simple and rapid micropatterning of conductive carbon composites and its application to elastic strain sensors. *Carbon* 2014;77:199-207. DOI
48. Chen Z, Ren W, Gao L, Liu B, Pei S, Cheng HM. Three-dimensional flexible and conductive interconnected graphene networks grown by chemical vapour deposition. *Nat Mater* 2011;10:424-8. DOI PubMed
49. Boland CS, Khan U, Ryan G, et al. Sensitive electromechanical sensors using viscoelastic graphene-polymer nanocomposites. *Science* 2016;354:1257-60. DOI
50. Kabiri Ameri S, Ho R, Jang H, et al. Graphene electronic tattoo sensors. *ACS Nano* 2017;11:7634-41. DOI
51. Lee WH, Suk JW, Lee J, et al. Simultaneous transfer and doping of CVD-grown graphene by fluoropolymer for transparent conductive films on plastic. *ACS Nano* 2012;6:1284-90. DOI
52. Sekitani T, Nakajima H, Maeda H, et al. Stretchable active-matrix organic light-emitting diode display using printable elastic conductors. *Nat Mater* 2009;8:494-9. DOI PubMed
53. Han L, Liu K, Wang M, et al. Mussel-inspired adhesive and conductive hydrogel with long-lasting moisture and extreme temperature tolerance. *Adv Funct Mater* 2018;28:1704195. DOI
54. Lipomi DJ, Vosgueritchian M, Tee BC, et al. Skin-like pressure and strain sensors based on transparent elastic films of carbon nanotubes. *Nat Nanotechnol* 2011;6:788-92. DOI
55. Ray TR, Choi J, Bandodkar AJ, et al. Bio-integrated wearable systems: a comprehensive review. *Chem Rev* 2019;119:5461-533. DOI
56. Wang C, Xia K, Wang H, Liang X, Yin Z, Zhang Y. Advanced carbon for flexible and wearable electronics. *Adv Mater* 2019;31:e1801072. DOI
57. Hu L, Pasta M, Mantia FL, et al. Stretchable, porous, and conductive energy textiles. *Nano Lett* 2010;10:708-14. DOI
58. Qiu L, Liu D, Wang Y, et al. Mechanically robust, electrically conductive and stimuli-responsive binary network hydrogels enabled by superelastic graphene aerogels. *Adv Mater* 2014;26:3333-7. DOI
59. Tringides CM, Vachicouras N, de Lázaro I, et al. Viscoelastic surface electrode arrays to interface with viscoelastic tissues. *Nat Nanotechnol* 2021;16:1019-29. DOI PubMed PMC
60. Polat EO, Balci O, Kakenov N, Uzlu HB, Kocabas C, Dahiya R. Synthesis of large area graphene for high performance in flexible optoelectronic devices. *Sci Rep* 2015;5:16744. DOI PubMed PMC
61. Gan D, Huang Z, Wang X, et al. Graphene oxide-templated conductive and redox-active nanosheets incorporated hydrogels for adhesive bioelectronics. *Adv Funct Mater* 2020;30:1907678. DOI
62. Xia S, Song S, Jia F, Gao G. A flexible, adhesive and self-healable hydrogel-based wearable strain sensor for human motion and physiological signal monitoring. *J Mater Chem B* 2019;7:4638-48. DOI
63. Ojha S, Acharya SK, Raghavendra G. Mechanical properties of natural carbon black reinforced polymer composites. *J Appl Polym Sci* 2015:132. DOI
64. Kim KS, Zhao Y, Jang H, et al. Large-scale pattern growth of graphene films for stretchable transparent electrodes. *Nature* 2009;457:706-10. DOI
65. Nair RR, Blake P, Grigorenko AN, et al. Fine structure constant defines visual transparency of graphene. *Science* 2008;320:1308. DOI
66. Lee H, Lee Y, Song C, et al. An endoscope with integrated transparent bioelectronics and theranostic nanoparticles for colon cancer

treatment. *Nat Commun* 2015;6:10059. DOI PubMed PMC
67. Liu N, Chortos A, Lei T, et al. Ultratransparent and stretchable graphene electrodes. *Sci Adv* 2017;3:e1700159. DOI PubMed PMC
68. Shi G, Lowe SE, Teo AJ, et al. A versatile PDMS submicrobead/graphene oxide nanocomposite ink for the direct ink writing of wearable micron-scale tactile sensors. *Appl Mater Today* 2019;16:482-92. DOI
69. Sun Y, Li D, Kim JU, et al. Carbon aerogel reinforced PDMS nanocomposites with controllable and hierarchical microstructures for multifunctional wearable devices. *Carbon* 2021;171:758-67. DOI
70. Wu J, Wang H, Su Z, et al. Highly flexible and sensitive wearable e-skin based on graphite nanoplatelet and polyurethane nanocomposite films in mass industry production available. *ACS Appl Mater Interfaces* 2017;9:38745-54. DOI
71. Amjadi M, Turan M, Clementson CP, Sitti M. Parallel microcracks-based ultrasensitive and highly stretchable strain sensors. *ACS Appl Mater Interfaces* 2016;8:5618-26. DOI PubMed
72. Sekitani T, Noguchi Y, Hata K, Fukushima T, Aida T, Someya T. A rubberlike stretchable active matrix using elastic conductors. *Science* 2008;321:1468-72. DOI PubMed
73. Gu X, Li S, Xiao Y, et al. Exposure to black carbon is associated with dermographism: a population-based study in college students. *Australas J Dermatol* 2022;63:e86-8. DOI PubMed
74. Serup J. How to diagnose and classify tattoo complications in the clinic: a system of distinctive patterns. In: Serup J, Bäumler W, editors. Diagnosis and Therapy of Tattoo Complications. S. Karger AG; 2017. p. 58-73. DOI
75. Fusco L, Garrido M, Martín C, et al. Skin irritation potential of graphene-based materials using a non-animal test. *Nanoscale* 2020;12:610-22. DOI
76. Ema M, Matsuda A, Kobayashi N, Naya M, Nakanishi J. Evaluation of dermal and eye irritation and skin sensitization due to carbon nanotubes. *Regul Toxicol Pharmacol* 2011;61:276-81. DOI PubMed
77. Liu Y, Feig VR, Bao Z. Conjugated polymer for implantable electronics toward clinical application. *Adv Healthc Mater* 2021;10:e2001916. DOI PubMed
78. Green RA, Baek S, Poole-Warren LA, Martens PJ. Conducting polymer-hydrogels for medical electrode applications. *Sci Technol Adv Mater* 2010;11:014107. DOI PubMed PMC
79. Wang S, Xu J, Wang W, et al. Skin electronics from scalable fabrication of an intrinsically stretchable transistor array. *Nature* 2018;555:83-8. DOI PubMed
80. Nezakati T, Seifalian A, Tan A, Seifalian AM. Conductive polymers: opportunities and challenges in biomedical applications. *Chem Rev* 2018;118:6766-843. DOI PubMed
81. Wang Y, Zhu C, Pfattner R, et al. A highly stretchable, transparent, and conductive polymer. *Sci Adv* 2017;3:e1602076. DOI PubMed PMC
82. Deslouis C, El Moustafid T, Musiani M, Tribollet B. Mixed ionic-electronic conduction of a conducting polymer film. Ac impedance study of polypyrrole. *Electrochimica Acta* 1996;41:1343-9. DOI
83. Tan P, Wang H, Xiao F, et al. Solution-processable, soft, self-adhesive, and conductive polymer composites for soft electronics. *Nat Commun* 2022;13:358. DOI PubMed PMC
84. Fang B, Yan J, Chang D, et al. Scalable production of ultrafine polyaniline fibres for tactile organic electrochemical transistors. *Nat Commun* 2022;13:2101. DOI PubMed PMC
85. Feig VR, Tran H, Lee M, Bao Z. Mechanically tunable conductive interpenetrating network hydrogels that mimic the elastic moduli of biological tissue. *Nat Commun* 2018;9:2740. DOI PubMed PMC
86. Liu Y, Liu J, Chen S, et al. Soft and elastic hydrogel-based microelectronics for localized low-voltage neuromodulation. *Nat Biomed Eng* 2019;3:58-68. DOI PubMed
87. Jiang Y, Zhang Z, Wang YX, et al. Topological supramolecular network enabled high-conductivity, stretchable organic bioelectronics. *Science* 2022;375:1411-7. DOI
88. Pomfret SJ, Adams PN, Comfort NP, Monkman AP. Inherently electrically conductive fibers wet spun from a sulfonic acid-doped polyaniline solution. *Adv Mater* 1998;10:1351-3. DOI
89. Cho S, Lee JS, Joo H. Recent developments of the solution-processable and highly conductive polyaniline composites for optical and electrochemical applications. *Polymers* 2019;11:1965. DOI PubMed PMC
90. Wang Y, Shi Y, Pan L, et al. Dopant-enabled supramolecular approach for controlled synthesis of nanostructured conductive polymer hydrogels. *Nano Lett* 2015;15:7736-41. DOI
91. Humpolicek P, Kasparkova V, Saha P, Stejskal J. Biocompatibility of polyaniline. *Synthetic Metals* 2012;162:722-7. DOI
92. Lalegül-ülker Ö, Elçin AE, Elçin YM. Intrinsically conductive polymer nanocomposites for cellular applications. In: Chun HJ, Park CH, Kwon IK, Khang G, editors. Cutting-Edge Enabling Technologies for Regenerative Medicine. Singapore: Springer; 2018. p. 135-53. DOI
93. Choi S, Park J, Hyun W, et al. Stretchable heater using ligand-exchanged silver nanowire nanocomposite for wearable articular thermotherapy. *ACS Nano* 2015;9:6626-33. DOI
94. Ma R, Kang B, Cho S, Choi M, Baik S. Extraordinarily high conductivity of stretchable fibers of polyurethane and silver nanoflowers. *ACS Nano* 2015;9:10876-86. DOI PubMed
95. Miyamoto A, Lee S, Cooray NF, et al. Inflammation-free, gas-permeable, lightweight, stretchable on-skin electronics with nanomeshes. *Nat Nanotechnol* 2017;12:907-13. DOI
96. Zhang A, Lee JH, Lieber CM. Nanowire-enabled bioelectronics. *Nano Today* 2021;38:101135. DOI PubMed PMC

97. Kim Y, Zhu J, Yeom B, et al. Stretchable nanoparticle conductors with self-organized conductive pathways. *Nature* 2013;500:59-63. DOI
98. Hyun DC, Park M, Park C, et al. Ordered zigzag stripes of polymer gel/metal nanoparticle composites for highly stretchable conductive electrodes. *Adv Mater* 2011;23:2946-50. DOI
99. Ma R, Lee J, Choi D, Moon H, Baik S. Knitted fabrics made from highly conductive stretchable fibers. *Nano Lett* 2014;14:1944-51. DOI PubMed
100. Liang J, Tong K, Pei Q. A water-based silver-nanowire screen-print ink for the fabrication of stretchable conductors and wearable thin-film transistors. *Adv Mater* 2016;28:5986-96. DOI PubMed
101. Jiang Z, Nayeem MOG, Fukuda K, et al. Highly stretchable metallic nanowire networks reinforced by the underlying randomly distributed elastic polymer nanofibers via interfacial adhesion improvement. *Adv Mater* 2019;31:e1903446. DOI
102. McShan D, Ray PC, Yu H. Molecular toxicity mechanism of nanosilver. *J Food Drug Anal* 2014;22:116-27. DOI PubMed PMC
103. Lim G, Kwak SS, Kwon N, et al. Fully stretchable and highly durable triboelectric nanogenerators based on gold-nanosheet electrodes for self-powered human-motion detection. *Nano Energy* 2017;42:300-6. DOI
104. Gong S, Schwalb W, Wang Y, et al. A wearable and highly sensitive pressure sensor with ultrathin gold nanowires. *Nat Commun* 2014;5:3132. DOI
105. Yang M, Hood ZD, Yang X, Chi M, Xia Y. Facile synthesis of Ag@Au core-sheath nanowires with greatly improved stability against oxidation. *Chem Commun* 2017;53:1965-8. DOI PubMed
106. Lim C, Park C, Sunwoo SH, et al. Facile and scalable synthesis of whiskered gold nanosheets for stretchable, conductive, and biocompatible nanocomposites. *ACS Nano* 2022;16:10431-42. DOI
107. Choi S, Han SI, Jung D, et al. Highly conductive, stretchable and biocompatible Ag-Au core-sheath nanowire composite for wearable and implantable bioelectronics. *Nat Nanotechnol* 2018;13:1048-56. DOI PubMed
108. Paladini F, Sannino A, Pollini M. In vivo testing of silver treated fibers for the evaluation of skin irritation effect and hypoallergenicity. *J Biomed Mater Res B Appl Biomater* 2014;102:1031-7. DOI PubMed
109. Hadrup N, Sharma AK, Loeschner K. Toxicity of silver ions, metallic silver, and silver nanoparticle materials after in vivo dermal and mucosal surface exposure: a review. *Regul Toxicol Pharmacol* 2018;98:257-67. DOI PubMed
110. Bomhard EM. The toxicology of indium oxide. *Environ Toxicol Pharmacol* 2018;58:250-8. DOI PubMed
111. Roach KA, Anderson SE, Stefaniak AB, Shane HL, Boyce GR, Roberts JR. Evaluation of the skin-sensitizing potential of gold nanoparticles and the impact of established dermal sensitivity on the pulmonary immune response to various forms of gold. *Nanotoxicology* 2020;14:1096-117. DOI PubMed PMC
112. Gupta R, Rai B. Penetration of gold nanoparticles through human skin: unraveling its mechanisms at the molecular scale. *J Phys Chem B* 2016;120:7133-42. DOI PubMed
113. Daeneke T, Khoshmanesh K, Mahmood N, et al. Liquid metals: fundamentals and applications in chemistry. *Chem Soc Rev* 2018;47:4073-111. DOI
114. Wang H, Xing W, Chen S, Song C, Dickey MD, Deng T. Liquid metal composites with enhanced thermal conductivity and stability using molecular thermal linker. *Adv Mater* 2021;33:e2103104. DOI
115. Yan J, Lu Y, Chen G, Yang M, Gu Z. Advances in liquid metals for biomedical applications. *Chem Soc Rev* 2018;47:2518-33. DOI
116. Dickey MD. Stretchable and soft electronics using liquid metals. *Adv Mater* 2017;29:1606425. DOI PubMed
117. Li Y, Feng S, Cao S, Zhang J, Kong D. Printable liquid metal microparticle ink for ultrastretchable electronics. *ACS Appl Mater Interfaces* 2020;12:50852-9. DOI
118. Veerapandian S, Jang W, Seol JB, et al. Hydrogen-doped viscoplastic liquid metal microparticles for stretchable printed metal lines. *Nat Mater* 2021;20:533-40. DOI
119. Guymon GG, Malakooti MH. Multifunctional liquid metal polymer composites. *J Polym Sci* 2022;60:1300-27. DOI
120. Hoang TT, Phan PT, Thai MT, et al. Magnetically engineered conductivity of soft liquid metal composites for robotic, wearable electronic, and medical applications. *Adv Intell Syst* 2022;4:2200282. DOI
121. Fassler A, Majidi C. Liquid-phase metal inclusions for a conductive polymer composite. *Adv Mater* 2015;27:1928-32. DOI PubMed
122. Clarkson TW, Magos L, Myers GJ. The toxicology of mercury - current exposures and clinical manifestations. *N Engl J Med* 2003;349:1731-7. DOI PubMed
123. Kalantar-zadeh K, Rahim MA, Tang J. Low melting temperature liquid metals and their impacts on physical chemistry. *Acc Mater Res* 2021;2:577-80. DOI
124. Song H, Kim T, Kang S, Jin H, Lee K, Yoon HJ. Ga-based liquid metal micro/nanoparticles: recent advances and applications. *Small* 2020;16:1903391. DOI
125. Malakooti MH, Bockstaller MR, Matyjaszewski K, Majidi C. Liquid metal nanocomposites. *Nanoscale Adv* 2020;2:2668-77. DOI PubMed PMC
126. Lin Y, Cooper C, Wang M, Adams JJ, Genzer J, Dickey MD. Handwritten, soft circuit boards and antennas using liquid metal nanoparticles. *Small* 2015;11:6397-403. DOI PubMed
127. Boley JW, White EL, Kramer RK. Mechanically sintered gallium-indium nanoparticles. *Adv Mater* 2015;27:2355-60. DOI PubMed
128. Liu S, Yuen MC, White EL, et al. Laser sintering of liquid metal nanoparticles for scalable manufacturing of soft and flexible electronics. *ACS Appl Mater Interfaces* 2018;10:28232-41. DOI
129. Deng B, Cheng GJ. Pulsed laser modulated shock transition from liquid metal nanoparticles to mechanically and thermally robust

solid-liquid patterns. *Adv Mater* 2019;31:e1807811. DOI PubMed

130. Xu Y, Lin Z, Rajavel K, et al. Tailorable, lightweight and superelastic liquid metal monoliths for multifunctional electromagnetic interference shielding. *Nanomicro Lett* 2021;14:29. DOI PubMed PMC
131. Markvicka EJ, Bartlett MD, Huang X, Majidi C. An autonomously electrically self-healing liquid metal-elastomer composite for robust soft-matter robotics and electronics. *Nat Mater* 2018;17:618-24. DOI PubMed
132. Mou L, Qi J, Tang L, et al. Highly stretchable and biocompatible liquid metal-elastomer conductors for self-healing electronics. *Small* 2020;16:e2005336. DOI PubMed
133. Liu S, Shah DS, Kramer-Bottiglio R. Highly stretchable multilayer electronic circuits using biphasic gallium-indium. *Nat Mater* 2021;20:851-8. DOI PubMed
134. Zhao Y, Huang X. Mechanisms and materials of flexible and stretchable skin sensors. *Micromachines* 2017;8:69. DOI PMC
135. Xu Y, Guo W, Zhou S, et al. Bioinspired perspiration-wicking electronic skins for comfortable and reliable multimodal health monitoring. *Adv Funct Materials* 2022;32:2200961. DOI
136. Liu S, Rao Y, Jang H, Tan P, Lu N. Strategies for body-conformable electronics. *Matter* 2022;5:1104-36. DOI
137. Ma Z, Huang Q, Xu Q, et al. Permeable superelastic liquid-metal fibre mat enables biocompatible and monolithic stretchable electronics. *Nat Mater* 2021;20:859-68. DOI
138. Park JE, Kang HS, Baek J, et al. Rewritable, printable conducting liquid metal hydrogel. *ACS Nano* 2019;13:9122-30. DOI
139. Jiang Y, Ji S, Sun J, et al. A universal interface for plug-and-play assembly of stretchable devices. *Nature* 2023;614:456-62. DOI
140. Kim JJ, Wang Y, Wang H, Lee S, Yokota T, Someya T. Skin electronics: next-generation device platform for virtual and augmented reality. *Adv Funct Mater* 2021;31:2009602. DOI
141. Choi C, Choi MK, Hyeon T, Kim D. Nanomaterial-based soft electronics for healthcare applications. *ChemNanoMat* 2016;2:1006-17. DOI
142. Zheng Z, Xia J, Wang B, Guo Y. Hierarchically designed nanocomposites for triboelectric nanogenerator toward biomechanical energy harvester and smart home system. *Nano Energy* 2022;95:107047. DOI
143. Lee Y, Kim J, Joo H, Raj MS, Ghaffari R, Kim D. Wearable sensing systems with mechanically soft assemblies of nanoscale materials. *Adv Mater Technol* 2017;2:1700053. DOI
144. Wang C, He K, Li J, Chen X. Conformal electrodes for on-skin digitalization. *SmartMat* 2021;2:252-62. DOI
145. Kwak SS, Yoo S, Avila R, et al. Skin-integrated devices with soft, holey architectures for wireless physiological monitoring, with applications in the neonatal intensive care unit. *Adv Mater* 2021;33:e2103974. DOI PubMed
146. Xiang L, Zeng X, Xia F, Jin W, Liu Y, Hu Y. Recent advances in flexible and stretchable sensing systems: from the perspective of system integration. *ACS Nano* 2020;14:6449-69. DOI
147. Tang L, Wu S, Qu J, Gong L, Tang J. A review of conductive hydrogel used in flexible strain sensor. *Materials* 2020;13:3947. DOI PubMed PMC
148. Ge J, Sun L, Zhang FR, et al. A stretchable electronic fabric artificial skin with pressure-, lateral strain-, and flexion-sensitive properties. *Adv Mater* 2016;28:722-8. DOI
149. Ha KH, Zhang W, Jang H, et al. Highly sensitive capacitive pressure sensors over a wide pressure range enabled by the hybrid responses of a highly porous nanocomposite. *Adv Mater* 2021;33:e2103320. DOI
150. Choi J, Ghaffari R, Baker LB, Rogers JA. Skin-interfaced systems for sweat collection and analytics. *Sci Adv* 2018;4:eaar3921. DOI PubMed PMC
151. Jang H, Sel K, Kim E, et al. Graphene e-tattoos for unobstructive ambulatory electrodermal activity sensing on the palm enabled by heterogeneous serpentine ribbons. *Nat Commun* 2022;13:6604. DOI PubMed PMC
152. Zhang L, Kumar KS, He H, et al. Fully organic compliant dry electrodes self-adhesive to skin for long-term motion-robust epidermal biopotential monitoring. *Nat Commun* 2020;11:4683. DOI PubMed PMC
153. Kim D, Rogers JA. Stretchable electronics: materials strategies and devices. *Adv Mater* 2008;20:4887-92. DOI
154. Lee GH, Woo H, Yoon C, et al. A personalized electronic tattoo for healthcare realized by on-the-spot assembly of an intrinsically conductive and durable liquid-metal composite. *Adv Mater* 2022;34:2270236. DOI
155. Yao S, Zhou W, Hinson R, et al. Ultrasoft porous 3D conductive dry electrodes for electrophysiological sensing and myoelectric control. *Adv Mater Technol* 2022;7:2101637. DOI PubMed PMC
156. Li Y, Yang D, Wu Z, et al. Self-adhesive, self-healing, biocompatible and conductive polyacrylamide nanocomposite hydrogels for reliable strain and pressure sensors. *Nano Energy* 2023;109:108324. DOI
157. Huang F, Wei W, Fan Q, Li L, Zhao M, Zhou Z. Super-stretchable and adhesive cellulose nanofiber-reinforced conductive nanocomposite hydrogel for wearable motion-monitoring sensor. *J Colloid Interface Sci* 2022;615:215-26. DOI
158. Lee JH, Hwang JY, Zhu J, et al. Flexible conductive composite integrated with personal earphone for wireless, real-time monitoring of electrophysiological signs. *ACS Appl Mater Interfaces* 2018;10:21184-90. DOI
159. Bayoumy K, Gaber M, Elshafeey A, et al. Smart wearable devices in cardiovascular care: where we are and how to move forward. *Nat Rev Cardiol* 2021;18:581-99. DOI PubMed PMC
160. Ershad F, Thukral A, Yue J, et al. Ultra-conformal drawn-on-skin electronics for multifunctional motion artifact-free sensing and point-of-care treatment. *Nat Commun* 2020;11:3823. DOI PubMed PMC
161. Zu W, Ohm Y, Carneiro MR, Vinciguerra M, Tavakoli M, Majidi C. A comparative study of silver microflakes in digitally printable liquid metal embedded elastomer inks for stretchable electronics. *Adv Mater Technol* 2022;7:2200534. DOI

162. Namkoong M, Guo H, Rahman MS, et al. Moldable and transferrable conductive nanocomposites for epidermal electronics. *Npj Flex Electron* 2022;6:41. DOI PubMed PMC
163. Roberts P, Zadan M, Majidi C. Soft tactile sensing skins for robotics. *Curr Robot Rep* 2021;2:343-54. DOI
164. Feng Y, Yu J, Sun D, Ren W, Shao C, Sun R. Solvent-induced in-situ self-assembly lignin nanoparticles to reinforce conductive nanocomposite organogels as anti-freezing and anti-dehydration flexible strain sensors. *Chem Eng J* 2022;433:133202. DOI
165. Li S, Xiao X, Hu J, et al. Recent advances of carbon-based flexible strain sensors in physiological signal monitoring. *ACS Appl Electron Mater* 2020;2:2282-300. DOI
166. Zhou Y, Lian H, Li Z, et al. Crack engineering boosts the performance of flexible sensors. *VIEW* 2022;3:20220025. DOI
167. Sun H, Fang X, Fang Z, et al. An ultrasensitive and stretchable strain sensor based on a microcrack structure for motion monitoring. *Microsyst Nanoeng* 2022;8:111. DOI PubMed PMC
168. Wang S, Xiao P, Liang Y, et al. Network cracks-based wearable strain sensors for subtle and large strain detection of human motions. *J Mater Chem C* 2018;6:5140-7. DOI
169. Amjadi M, Pichitpajongkit A, Lee S, Ryu S, Park I. Highly stretchable and sensitive strain sensor based on silver nanowire-elastomer nanocomposite. *ACS Nano* 2014;8:5154-63. DOI PubMed
170. Stoyanov H, Kollosche M, Risse S, Waché R, Kofod G. Soft conductive elastomer materials for stretchable electronics and voltage controlled artificial muscles. *Adv Mater* 2013;25:578-83. DOI PubMed
171. Lee H, Kwon D, Cho H, Park I, Kim J. Soft nanocomposite based multi-point, multi-directional strain mapping sensor using anisotropic electrical impedance tomography. *Sci Rep* 2017;7:39837. DOI PubMed PMC
172. Araromi OA, Graule MA, Dorsey KL, et al. Ultra-sensitive and resilient compliant strain gauges for soft machines. *Nature* 2020;587:219-24. DOI
173. Yun T, Du J, Ji X, et al. Waterproof and ultrasensitive paper-based wearable strain/pressure sensor from carbon black/multilayer graphene/carboxymethyl cellulose composite. *Carbohydr Polym* 2023;313:120898. DOI
174. Hasan MR, Sharma P, Suleman S, et al. Papertronics: marriage between paper and electronics becoming a real scenario in resource-limited settings. *ACS Appl Bio Mater* 2023;6:1368-79. DOI
175. Solak İ, Gençer Ş, Yıldırım B, Öznur E, Hah D, Icoz K. Respiration monitoring using a paper-based wearable humidity sensor, a step forward to clinical tests. *Sens Actuator A Phys* 2023;355:114316. DOI
176. Li T, Sakthivelpathi V, Qian Z, et al. Ultrasensitive capacitive sensor composed of nanostructured electrodes for human-machine interface. *Adv Mater Technol* 2022;7:2101704. DOI
177. Zhang J, Goodman SM, Wise HG, Dichiara AB, Chung J. Electromechanical coupling of isotropic fibrous networks with tailored auxetic behavior induced by water-printing under tension. *J Mater Chem C* 2021;9:4544-53. DOI
178. Lee J, Kwon H, Seo J, et al. Conductive fiber-based ultrasensitive textile pressure sensor for wearable electronics. *Adv Mater* 2015;27:2433-9. DOI
179. Su X, Wu X, Chen S, et al. A highly conducting polymer for self-healable, printable, and stretchable organic electrochemical transistor arrays and near hysteresis-free soft tactile sensors. *Adv Mater* 2022;34:2200682. DOI
180. Yang T, Deng W, Chu X, et al. Hierarchically microstructure-bioinspired flexible piezoresistive bioelectronics. *ACS Nano* 2021;15:11555-63. DOI
181. Yin T, Cheng Y, Hou Y, et al. 3D porous structure in MXene/PANI foam for a high-performance flexible pressure sensor. *Small* 2022;18:e2204806. DOI PubMed
182. Yang C, Li L, Zhao J, et al. Highly sensitive wearable pressure sensors based on three-scale nested wrinkling microstructures of polypyrrole films. *ACS Appl Mater Interfaces* 2018;10:25811-8. DOI
183. Wang D, Zhou X, Song R, et al. Freestanding silver/polypyrrole composite film for multifunctional sensor with biomimetic micropattern for physiological signals monitoring. *Chem Eng J* 2021;404:126940. DOI
184. Kwon K, Kim JU, Won SM, et al. A battery-less wireless implant for the continuous monitoring of vascular pressure, flow rate and temperature. *Nat Biomed Eng* 2023. DOI
185. Li AL, Zhu S, Hu ZH, Peng Q, Fang X, Zhang YY. The distribution and epidemic characteristics of cerebrovascular disease in followed-up hypertension patients. *Sci Rep* 2021;11:9366. DOI PubMed PMC
186. Jaffey JA, Wiggen K, Leach SB, Masseau I, Girens RE, Reinero CR. Pulmonary hypertension secondary to respiratory disease and/or hypoxia in dogs: clinical features, diagnostic testing and survival. *Vet J* 2019;251:105347. DOI PubMed
187. Luo N, Dai W, Li C, et al. Flexible piezoresistive sensor patch enabling ultralow power cuffless blood pressure measurement. *Adv Funct Mater* 2016;26:1178-87. DOI
188. Lou Y, Liu H, Zhang J. Liquid metals in plastics for super-toughness and high-performance force sensors. *Chem Eng J* 2020;399:125732. DOI
189. Ning C, Dong K, Cheng R, et al. Flexible and stretchable fiber-shaped triboelectric nanogenerators for biomechanical monitoring and human-interactive sensing. *Adv Funct Mater* 2021;31:2006679. DOI
190. Liu Y, Yu Q, Luo X, Yang L, Cui Y. Continuous monitoring of diabetes with an integrated microneedle biosensing device through 3D printing. *Microsyst Nanoeng* 2021;7:75. DOI PubMed PMC
191. Bakker J, Nijsten MW, Jansen TC. Clinical use of lactate monitoring in critically ill patients. *Ann Intensive Care* 2013;3:12. DOI PubMed PMC
192. Pirovano P, Dorrian M, Shinde A, et al. A wearable sensor for the detection of sodium and potassium in human sweat during

exercise. *Talanta* 2020;219:121145. DOI

193. Lee H, Hong YJ, Baik S, Hyeon T, Kim DH. Enzyme-based glucose sensor: from invasive to wearable device. *Adv Healthc Mater* 2018;7:e1701150. DOI PubMed
194. Zhai Q, Yap LW, Wang R, et al. Vertically aligned gold nanowires as stretchable and wearable epidermal ion-selective electrode for noninvasive multiplexed sweat analysis. *Anal Chem* 2020;92:4647-55. DOI
195. Oh SY, Hong SY, Jeong YR, et al. Skin-attachable, stretchable electrochemical sweat sensor for glucose and pH detection. *ACS Appl Mater Interfaces* 2018;10:13729-40. DOI
196. Garg V, Gupta T, Rani S, et al. A hierarchically designed nanocomposite hydrogel with multisensory capabilities towards wearable devices for human-body motion and glucose concentration detection. *Compos Sci Technol* 2021;213:108894. DOI
197. Shu Y, Su T, Lu Q, Shang Z, Xu Q, Hu X. Highly stretchable wearable electrochemical sensor based on Ni-Co MOF nanosheet-decorated Ag/rGO/PU fiber for continuous sweat glucose detection. *Anal Chem* 2021;93:16222-30. DOI PubMed
198. Chandran N, Janardhanan P, Bayal M, Pilankatta R, Nair SS. Development of a paper printed colorimetric sensor based on Cu-Curcumin nanoparticles for evolving point-of-care clinical diagnosis of sodium. *Sci Rep* 2022;12:6247. DOI PubMed PMC
199. Lim H, Lee Y, Jones KA, et al. All-in-one, wireless, fully flexible sodium sensor system with integrated Au/CNT/Au nanocomposites. *Sens Actuators B Chem* 2021;331:129416. DOI
200. Khalid MAU, Chang SH. Flexible strain sensors for wearable applications fabricated using novel functional nanocomposites: a review. *Compos Struct* 2022;284:115214. DOI
201. Said RAM, Hasan MA, Abdelzaher AM, Abdel-raoof AM. Review - insights into the developments of nanocomposites for its processing and application as sensing materials. *J Electrochem Soc* 2020;167:037549. DOI
202. Shameem M, Sasikanth S, Annamalai R, Ganapathi Raman R. A brief review on polymer nanocomposites and its applications. *Mater Today* 2021;45:2536-9. DOI
203. Guo L, Ma M, Zhang N, Langer R, Anderson DG. Stretchable polymeric multielectrode array for conformal neural interfacing. *Adv Mater* 2014;26:1427-33. DOI PubMed PMC
204. Li Y, Gao Y, Lan L, et al. Ultrastretchable and wearable conductive multifilament enabled by buckled polypyrrole structure in parallel. *npj Flex Electron* 2022;6:42. DOI
205. Guan YS, Zhang Z, Tang Y, Yin J, Ren S. Kirigami-inspired nanoconfined polymer conducting nanosheets with 2000% stretchability. *Adv Mater* 2018;30:1706390. DOI